Journal of Neurochemistry JNC

JOURNAL OF NEUROCHEMISTRY | 2011 | 116 | 76–81 doi: 10.1111/j.1471-4159.2010.07086.x

Polypyrimidine tract-binding protein 1 regulates the alternative splicing of dopamine receptor D_2

Toshikazu Sasabe,*,† Eugene Futai* and Shoichi Ishiura*

*Department of Life Sciences, Graduate School of Arts and Sciences, The University of Tokyo, Tokyo, Japan

†Research Fellowships of the Japan Society for the Promotion of Science for Young Scientists

Abstract

Dopamine receptor D_2 (DRD2) has two splicing isoforms, a long form (D2L) and short form (D2S), which have distinct functions in the dopaminergic system. However, the regulatory mechanism of the alternative splicing of *DRD2* is unknown. In this study, we examined which splicing factors regulate the expression of D2L and D2S by over-expressing several RNA-binding proteins in HEK293 cells. In a cellular splicing assay, the over-expression of polypyrimidine tract-binding protein 1 (PTBP1) reduced the expression of D2S, whereas the knockdown of PTBP1 increased the expression of D2S. We also identified the regions of *DRD2* that are responsive to PTBP1 using heterologous minigenes and deletion mutants. Our results indicate that PTBP1 regulates the alternative splicing of *DRD2*. Considering that DRD2 inhibits cAMP-dependent protein kinase A, which modulates the intracellular localization of PTBP1, PTBP1 may contribute to the autoregulation of DRD2 by regulating the expression of its isoforms.

Keywords: alternative splicing, dopamine, dopamine receptor D_2, PTBP1.

J. Neurochem. (2011) **116**, 76–81.

Dopamine is the predominant neurotransmitter in the CNS, where it plays a leading role in the regulation of such physiological functions as locomotor activity, cognition, positive reinforcement, and hormone secretion. The effects of dopamine are mediated by its binding to five G-protein-coupled receptors, which are divided into two subclasses: D_1-like (D_1 and D_5) and D_2-like (D_2, D_3, and D_4). Dopamine receptor D_2 (DRD2) is the main autoreceptor of the dopaminergic system (Centonze *et al.* 2002); however, it is also critical for post-synaptic transmission (Usiello *et al.* 2000).

Alternative gene splicing generates two distinct isoforms of DRD2, a long form (D2L) and short form (D2S), which differ in the presence of a 29-amino-acid insert in the third cytoplasmic loop. D2L is expressed mainly in post-synaptic regions, whereas D2S is expressed mainly in pre-synaptic regions (Khan *et al.* 1998; Usiello *et al.* 2000). These isoforms differentially contribute to the pre-synaptic inhibition of glutamate and GABA transmission (Centonze *et al.* 2004); moreover, they exhibit specific G_i protein preferences (Senogles 1994; Guiramand *et al.* 1995; Senogles *et al.* 2004) and have distinct roles in the regulation of protein phosphorylation (Lindgren *et al.* 2003). Furthermore, behavioral studies of D2L-deficient mice have shown that D2L and D2S contribute differentially to the regulation of certain motor functions (Usiello *et al.* 2000; Wang *et al.* 2000) and emotional responses (Hranilovic *et al.* 2008). Similarly, human genetic studies have shown that the intronic single nucleotide polymorphism rs1076560, which has a significant effect on the expression ratio of the DRD2 isoforms, is associated with cognitive processing (Zhang *et al.* 2007) and emotional processing (Blasi *et al.* 2009). These results suggest that the expression ratio of the DRD2 isoforms is important for their functions.

However, little is known about the regulatory mechanism that mediates the alternative splicing of *DRD2*. Although it has been reported that haloperidol, sex steroid hormones, and ethanol affect the expression of splice variants (Arnauld *et al.* 1991; Guivarc'h *et al.* 1995, 1998; Oomizu *et al.* 2003), the molecular basis for these differences is unclear. In general, changes in splicing patterns are directed by regula-

Received August 26, 2010; revised manuscript received October 18, 2010; accepted October 22, 2010.

Address correspondence and reprint requests to Dr Shoichi Ishiura. Department of Life Sciences, Graduate School of Arts and Sciences, The University of Tokyo. 3-8-1, Komaba, Meguro-ku, Tokyo 153-8902, Japan. E-mail: cishiura@mail.ecc.u-tokyo.ac.jp

Abbreviations used: D2L, long form of DRD2; D2S, short form of DRD2; DRD2, dopamine receptor D_2; nPTB, neural PTB; PTBP1, polypyrimidine tract-binding protein 1; Tpm2, tropomyosin 2.

tory proteins that bind the pre-mRNA sequence and enhance or silence particular splicing choices (Li *et al.* 2007). Thus, in this study, we searched for proteins that regulate the alternative splicing of *DRD2* using a cellular splicing assay and identified the involvement of the splicing factor polypyrimidine tract-binding protein 1 (PTBP1).

Materials and methods

Plasmid construction

The region from exon 5 to exon 7 of *DRD2* was amplified from human genomic DNA and cloned into the *Xho*I-*Hind*III site of pEYFP-C1 (Clontech, Mountain View, CA, USA) (Fig. 1a). The open reading frames that encode SF2/ASF, PTBP1, nPTB, NOVA1, HuB, FOX2, hnRNP A1, and Tra2b were amplified by PCR from a human fetal brain cDNA library (Clontech) and cloned into pcDNA3.1/V5-His (Invitrogen, Carlsbad, CA, USA) using conventional biological techniques. Primer sequences are listed in Table S1. Plasmid constructions of NAPOR and FOX1 are gifts from Dr. Yoshihiro Kino, RIKEN Brain Science Institute, and hnRNP H from Dr. Kinji Ohno, Nagoya University. Heterologous minigenes were generated by inserting *DRD2* fragments containing exon 6, exon 7 and flanking regions into pEGFP-Tpm2-ex1-2 (a gift from Dr. Kino, RIKEN Brain Science Institute). *DRD2* deletion mutants were generated by inverse PCR from the wild-type plasmid using primers flanking the deleted regions. The nucleotide sequences of the DNA inserts were confirmed by sequencing.

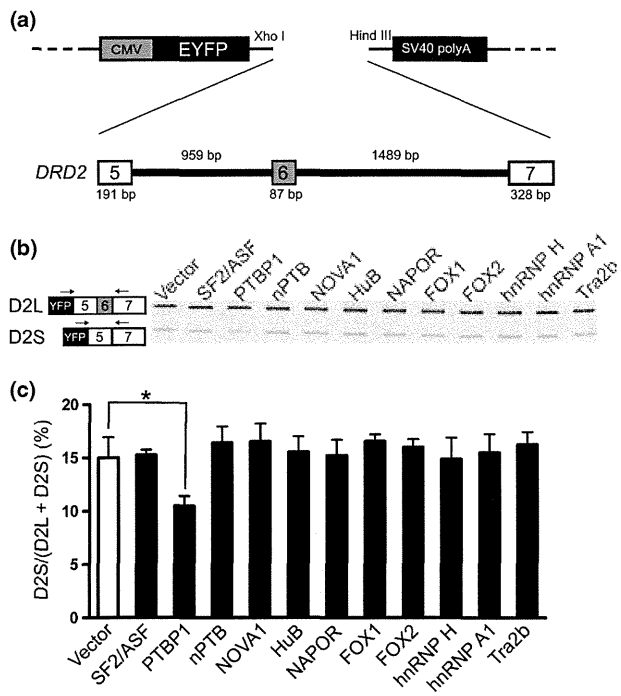

Fig. 1 The over-expression of PTBP1 reduced the alternative splicing of D2S. (a) Structure of the *DRD2* minigene. (b) Representative result from RT-PCR assays in which the *DRD2* minigene and plasmids for expressing RNA-binding proteins were transfected into HEK293 cells. The upper bands correspond to the splice product containing exon 6 (D2L), while the lower bands correspond to the splice product lacking exon 6 (D2S). (c) Bar chart showing the quantified percentage of D2S (Mean + SEM, $n = 3$). The statistical significance was analyzed by Dunnett's multiple-comparison test ($^*p < 0.05$).

Cell culture and transfection

HEK293 and SH-SY5Y cells were cultured in Dulbecco's modified Eagle's medium supplemented with 10% (v/v) fetal bovine serum and incubated at 37°C with 5% CO_2. For the minigene assays, HEK293 cells were transfected with plasmids for the expression of minigene and V5-tagged proteins using Fugene 6 (Roche Diagnostics, Basel, Switzerland). In our RNAi experiments, HEK293 cells were transfected with the minigene plasmids and an siRNA for *PTBP1* (Invitrogen, Stealth™ Select RNAi HSS143520, and Negative Control Hi GC) and *nPTB* (Invitrogen, Stealth™ Select RNAi HSS126818, and Negative Control Lo GC) using Lipofectamine 2000 (Invitrogen), and SH-SY5Y cells were transfected with the siRNA using Lipofectamine RNAiMAX (Invitrogen) and the Reverse Transfection protocol. The efficacy of the RNAi-mediated knockdown of endogenous PTBP1, nPTB, and actin expressions was determined by western blot analysis using anti-PTBP1 (Invitrogen, catalog No. 32-4800), anti-nPTB (Abnova, Taipei City, Taiwan, catalog No. H00058155-A01), and anti-actin (Sigma-Aldrich, St. Louis, MO, USA, catalog No. A2066) antibodies.

Identification of DRD2 splice variants

Forty-eight hours after transfection, total RNA was isolated from the cells using a GenElute Mammalian Total RNA Miniprep Kit (Sigma-Aldrich). cDNA synthesis was performed using a PrimeScript First Strand cDNA Synthesis Kit (TAKARA BIO, Shiga, Japan) using oligo dT primer. The DRD2 minigene fragments were amplified by PCR (20 cycles) using a forward primer specific for the 3′ region of *EYFP* (AAGTCCGGACTCAGATCTCG) and a *DRD2*-specific reverse primer (DRD2-Ex7-Rv) that annealed to the 5′ region of exon 7 (CATCTCCATCTCCAGCTCCT). To detect endogenous *DRD2* fragments, a forward primer specific for exons 4 and 5 (CAATAACGCAGACCAGAACG) and DRD2-Ex7-Rv were used (40 cycles). For tropomyosin 2 (Tpm2)-based minigenes, primers green fluorescence protein (GFP)-Fw (CATGGTCCTGCTGGAGTTCGTG) and Tpm2-ex2-splicing-Rv2 (GGAGGGCCTGCTGCTCTTC) were used (Kino *et al.* 2009). The amplified products were resolved by 6% polyacrylamide gel electrophoresis and visualized using ethidium bromide. The intensities of the bands corresponding to the long and short forms were quantified by LAS-3000 and MultiGage software (Fuji Film, Tokyo, Japan). The quantified values were divided by the number of base pairs.

Results

PTBP1 regulates the alternative splicing of DRD2

To identify trans-acting factors that regulate the alternative splicing of *DRD2*, we used RT-PCR to detect splice variants. We constructed a gene fragment encompassing exons 5 through 7 of human *DRD2* in the vector pEYFP (Fig. 1a). This minigene was then transfected into HEK293 cells, and the expression ratios of D2L and D2S were analyzed by

RT-PCR. When the *DRD2* minigene was transfected with empty pcDNA3.1, the percentage of D2S was about 15% (Fig. 1b and c). Next, we expressed V5-tagged versions of several proteins known to regulate pre-mRNA splicing in the nervous system (SF2/ASF, PTBP1, nPTB, NOVA1, HuB, NAPOR, FOX1, FOX2, hnRNP H, hnRNP A1, and Tra2b); notably, SF2/ASF was previously proposed to regulate the alternative splicing of *DRD2* (Oomizu *et al.* 2003). Among the proteins tested, only when PTBP1 was transfected with the *DRD2* minigene was the percentage of D2S significantly reduced (to about 10%; Fig. 1b and c). We have confirmed the expressions of each RNA-binding proteins by western blot analysis and noted that the abundance of nPTB, NAPOR, and FOX1 are low (Figure S1). In addition, we showed the effects of PTBP1 were concentration dependent (Figure S2).

Next, we knocked down endogenous PTBP1 expression using an siRNA to confirm the effect of PTBP1 on *DRD2* splicing. We first confirmed the efficacy of the siRNA in modulating the expression of the target protein by western blot analysis (Fig. 2b). The presence of two PTBP1 bands rather than one is most likely because of phosphorylation. (Grossman *et al.* 1998). When the *DRD2* minigene was transfected with an siRNA for *PTBP1*, the percentage of D2S was significantly increased compared to transfection with a control siRNA (Fig. 2a). We also examined the effect of the knockdown of nPTB, a homologue of PTBP1, because it was reported that appearance of some exons are affected by both PTBP1 and nPTB (Boutz *et al.* 2007). The knockdown of PTBP1 increased the expression of nPTB (Fig. 2b), consistent with the previous reports (Boutz *et al.* 2007; Makeyev *et al.* 2007). While endogenous nPTB level was remarkably low and the knockdown of nPTB by siRNA was not observed, the increase in nPTB expression by the knockdown of PTBP1 was clearly inhibited by a siRNA for nPTB (Fig. 2b). Even when the increase in nPTB was inhibited, the knockdown of PTBP1 still increased the production of D2S splice variant (Fig. 2a), suggesting that the increase in nPTB has little or no effect on the alternative splicing of DRD2. Furthermore, we examined whether PTBP1 regulates the alternative splicing of endogenous *DRD2* in human neuroblastoma SH-SY5Y cells. When the siRNA for *PTBP1* was transfected into SH-SY5Y cells, the percentage of endogenous D2S fragments was also increased (Fig. 2c and d).

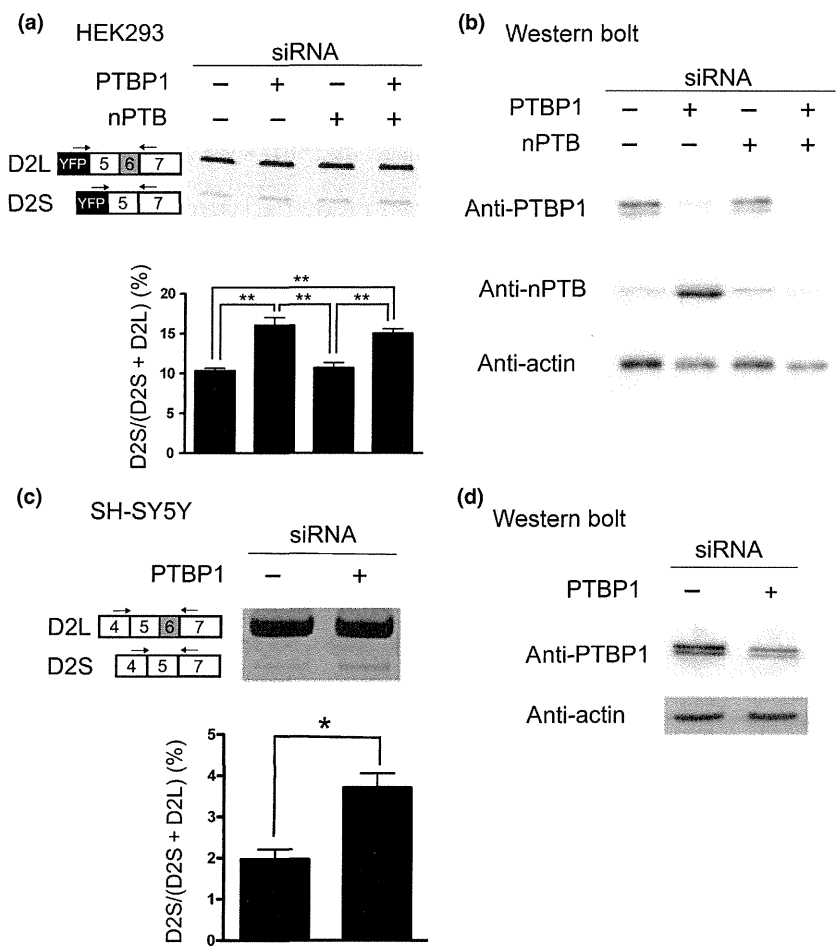

Fig. 2 The knockdown of PTBP1 increased the production of D2S splice variant. (a) Representative result from our cellular splicing assay using the *DRD2* minigene and siRNA for *PTBP1* and *nPTB* in HEK293 cells. Bar charts show the quantified percentages of D2S (Mean + SEM, $n = 3$). The statistical significances were analyzed using Tukey's multiple comparison test ($^{**}p < 0.01$). (b) Representative result of western blot analysis of PTBP1 and nPTB in HEK293 cells. (c) Representative result of endogenous *DRD2* splicing using a siRNA for *PTBP1* in SH-SY5Y cells. Bar charts show the quantified percentages of D2S (Mean + SEM, $n = 3$). The statistical significance was analyzed using *t*-tests ($^{*}p < 0.05$). (d) Representative result of western blot analysis of PTBP1 in SH-SY5Y cells.

Intronic regions flanking exon 6 are required for the PTBP1-mediated regulation of DRD2 splicing

To define the regions of *DRD2* that are required for its regulation by PTBP1, we utilized several previously generated heterologous minigenes (Kino *et al.* 2009). In these minigenes, the regions of interest were inserted in the context of constitutive exons of mouse *Tpm2*, which is distinct from *DRD2*. A reference fragment containing exon 9 of *Tpm2* and its flanking intronic regions or a *DRD2* fragment containing exon 6 or exon 7 and their flanking regions were inserted into a *Tpm2* fragment covering exons 1 and 2 (Fig. 3a). First, we

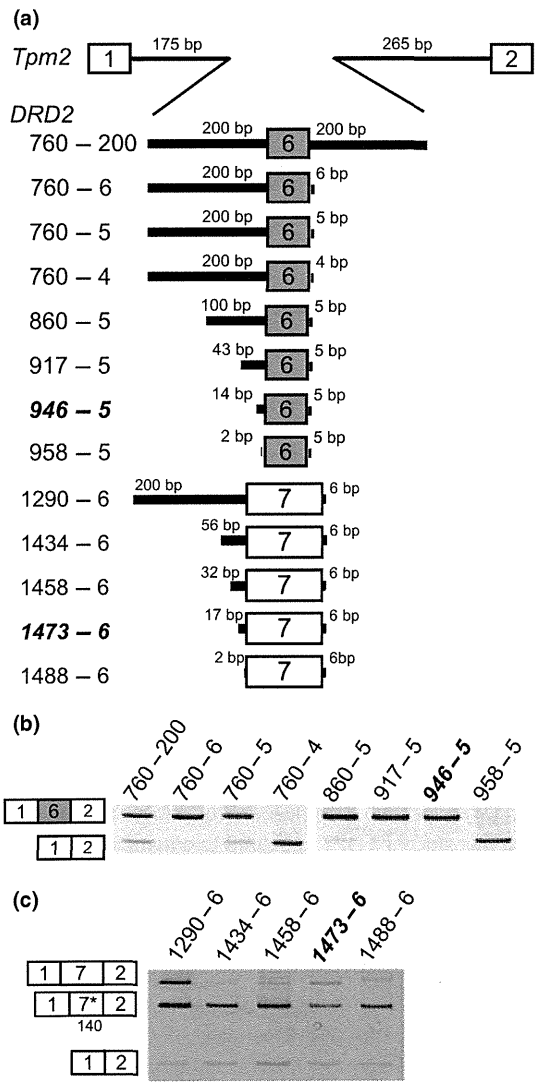

Fig. 3 Identification of DRD2 intronic regions which are necessary for the splicing of exon 6 and exon 7. (a) Structure of the *Tpm2*-based heterologous minigenes. The positions of the inserted nucleotides in introns 5, 6 and 7, as well as the numbers of base pairs in the fragments, are indicated. (b, c) Representative results from identification of splice variants using *Tpm2*-based heterologous minigenes in HEK293 cells. The white box 7* shows a shorter exon 7 lacking the first 140 nucleotides.

predicted branch sites by a web-based program called ESEfinder 3.0 (Table S2, http://rulai.cshl.edu/cgi-bin/tools/ESE3/esefinder.cgi). Then, using our *Tpm2*-based heterologous minigenes, we found that 14 bp upstream and 5 bp downstream of exon 6 are necessary for proper splicing (Fig. 3b). When exon 7 of DRD2 was inserted into Tpm2 cassette, a shorter exon 7 lacking the first 140 nucleotides was the main product. It was shown that 17 bp upstream of exon 7 is necessary for the splicing of full-length exon 7 (Fig. 3c). Because the primary elements regulating alternative splicing are thought to be located up to 200–300 nucleotides upstream and/or downstream of the regulated exon (Cooper 2005), a *DRD2* fragment stretching from 200 bp upstream of exon 6 (760 bp downstream of exon 5) to 200 bp downstream of exon 6 was used to examine the binding sequence of PTBP1 (Fig. 4a). PTBP1 had no effect on the inclusion of *Tpm2* exon 9 in HEK293 cells (Fig. 4b, left). In contrast, PTBP1 repressed *DRD2* exon 6 inclusion of the heterologous minigene, demonstrating that the inserted fragment of *DRD2* was sufficient for the response to PTBP1 (Fig. 4b, right). Next, to examine which region is necessary for the gene's responsiveness to PTBP1, we constructed *DRD2* deletion mutants lacking 200 bp upstream of exon 6 (Δint5_760–945), downstream of exon 6 (Δint6_6–200) or upstream of exon 7 (Δint6_1290–1487) (Fig. 4c). These deletion mutants were designed to include the regions that are necessary for splicing of exon 6 and exon 7. As shown in Fig. 4(d), Δint5_760–945 and Δint6_6–200 mutations altered the basal splicing pattern. Both deletion mutants exhibited markedly increased exclusion of exon 6 (from 15% to about 60% with vector transfection), suggesting the presence of elements in the deleted regions that enhance the inclusion of exon 6. Further, the over-expression of PTBP1 had no effect on either deletion mutant, indicating that both mutants had impaired responsiveness to PTBP1 (Fig. 4d). On the other hand, the over-expression of PTBP1 reduced D2S in the Δint6_1290–1487 mutant as well as a wild-type minigene, suggesting that PTBP1 affects the alternative splicing of DRD2 in regions other than the 3′ end of intron 6.

Discussion

Previous studies have shown that the functions of two splice variants of DRD2, D2L and D2S, differ in their biochemical properties and physiological functions (Senogles 1994; Guiramand *et al.* 1995; Khan *et al.* 1998; Usiello *et al.* 2000; Wang *et al.* 2000; Centonze *et al.* 2002, 2004; Lindgren *et al.* 2003; Senogles *et al.* 2004; Hranilovic *et al.* 2008); however, it is unclear what regulates the expression ratio of these isoforms. In this study, we identified PTBP1 as a splicing regulatory protein that reduces the expression of the D2S isoform.

Among the eleven proteins that we over-expressed with the *DRD2* minigene in HEK293 cells, only PTBP1

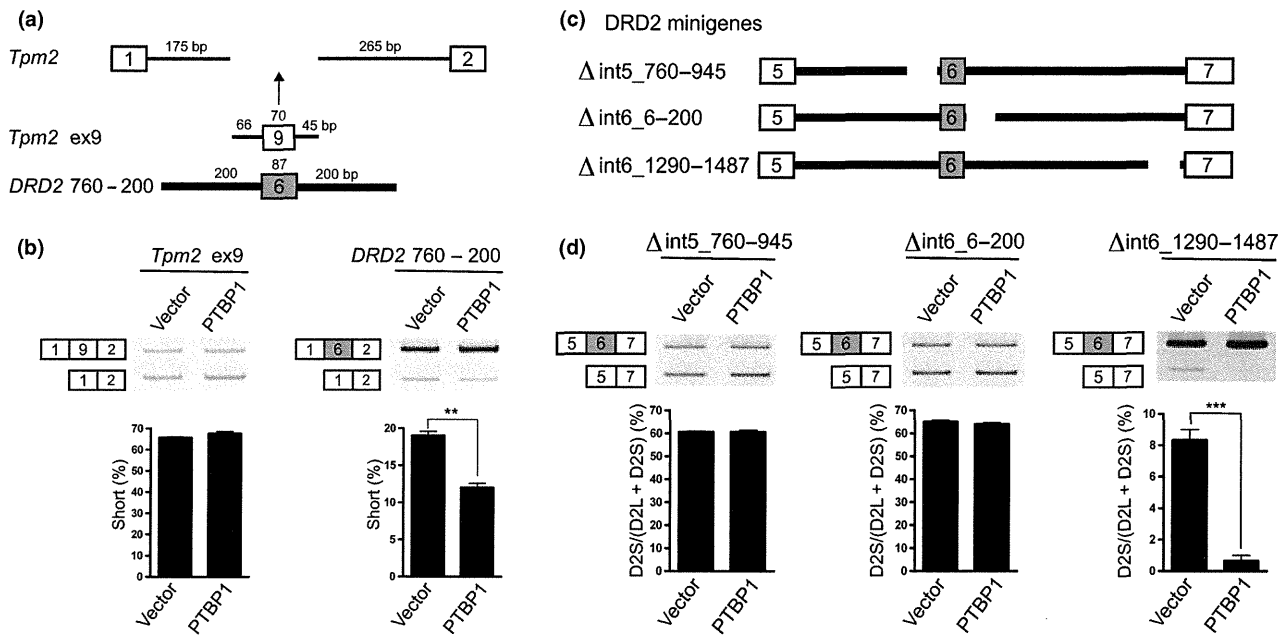

Fig. 4 Splicing regulation by PTBP1 in heterologous minigenes and *DRD2* deletion mutants. (a) Structure of the *Tpm2*-based heterologous minigene. Intronic fragments derived from *DRD2* are indicated by thick lines, whereas those derived from *Tpm2* are indicated by thin lines. (b) Splicing assay results using *Tpm2*-based heterologous minigenes and PTBP1 in HEK293 cells. Bar charts show the quantified percentages of exon exclusion (Mean + SEM, $n = 3$). (c) Structure of the *DRD2* deletion mutants. The positions of the inserted nucleotides in introns 5 and 6 are indicated. (d) Splicing assay results using the *DRD2* deletion mutants and PTBP1 in HEK293 cells. Bar charts show the quantified percentages of D2S (Mean + SEM, $n = 3$). The statistical significance was analyzed using *t*-tests (**$p < 0.01$, ***$p < 0.001$).

produced an altered splicing pattern (Fig. 1b and c). The reduction in the percentage of D2S suggests that PTBP1 enhances the inclusion of the alternative exon 6. Although the effect of PTBP1 was relatively small, this effect was shown to be concentration dependent (Figure S2). We also demonstrated that endogenous PTBP1 regulates DRD2 splicing by knockdown experiments in HEK293 cells with the *DRD2* minigene and in SH-SY5Y cells with the endogenous *DRD2* gene (Fig. 2a and c). Even though the effect of PTBP1 was statistically significant, it was quantitatively small in our splicing assay. Therefore, some other splicing factors may be involved in the splicing regulation of *DRD2*. In addition, the double knockdown of PTBP1 and nPTB suggested that nPTB, a homolog of PTBP1, has little or no effect on the alternative splicing of DRD2 (Fig. 2a). However, because the expression levels of exogenous and endogenous nPTB were remarkably lower than PTBP1 in HEK293 cells, it is still unclear whether nPTB regulates the splicing of DRD2.

Next, we identified the regions responsive to PTBP1, using *Tpm2*-based heterologous minigenes and *DRD2* deletion mutants. Using our heterologous minigenes, the splicing of a *DRD2* fragment containing exon 6 as well as 200 bp-upstream and -downstream intronic regions was altered by PTBP1 (Fig. 4b), similar to the results obtained using the *DRD2* minigene (Fig. 1b and c). In the *DRD2* deletion mutants, PTBP1 had no effect on the splicing of deletion mutants lacking exon 6-flanking regions in intron 5 or 6, whereas PTBP1 still affected the splicing of a deletion mutant lacking the 3′ end of intron 6 (Fig. 4d). These results indicate that exon 6-flanking regions are sufficient for the response to PTBP1, and that both regions in introns 5 and 6 are necessary.

Although PTBP1 is known to bind cytosine and uracil (CU)-rich intronic elements flanking an exon and repress splicing (Wagner and Garcia-Blanco 2001; Sharma *et al.* 2008), in this study PTBP1 appeared to enhance the inclusion of *DRD2* exon 6 rather than repressing the splicing from exon 5 to exon 7. It is noted that intron 5 contains UCUCU (849–853) and intron 6 contains UCUUUCU (32–38) sequences, but we have no evidence that PTBP1 directly binds the pre-mRNA of *DRD2*. Therefore it is possible that PTBP1 may indirectly affect the alternative splicing of *DRD2*.

It was reported that a DRD2 antagonist, haloperidol, increased the expression of D2S (Arnauld *et al.* 1991). The activation of DRD2 is coupled to the inhibition of adenylyl cyclase and cAMP-dependent protein kinase A, and cAMP-dependent protein kinase A has been shown to modulate the nucleocytoplasmic translocation of PTBP1 (Xie *et al.* 2003; Knoch *et al.* 2006). Together with these reports, our results suggest that DRD2 regulates the expression of its isoforms by modulating the localization of PTBP1.

Acknowledgements

This work was supported in part by the Human Frontier Science Program and by a Grant-in-Aid from the Ministry of Education, Culture, Sports, Science and Technology of Japan to S.I. T.S. is supported by a JSPS Research Fellowship for Young Scientists. We thank Dr. Yoshihiro Kino for Tpm2 minigene.

Supporting information

Additional Supporting information may be found in the online version of this article:

Figure S1. The expressions of RNA-binding proteins were confirmed by western blot analysis.

Figure S2. The concentration dependency of the PTBP1 effects.

Table S1. Primer sequences used for cloning.

Table S2. Branch site prediction by ESEfinder 3.0.

As a service to our authors and readers, this journal provides supporting information supplied by the authors. Such materials are peer-reviewed and may be re-organized for online delivery, but are not copy-edited or typeset. Technical support issues arising from supporting information (other than missing files) should be addressed to the authors.

References

Arnauld E., Arsaut J. and Demotes-Mainard J. (1991) Differential plasticity of the dopaminergic D2 receptor mRNA isoforms under haloperidol treatment, as evidenced by in situ hybridization in rat anterior pituitary. *Neurosci. Lett.* **130**, 12–16.

Blasi G., Lo Bianco L., Taurisano P. *et al.* (2009) Functional variation of the dopamine D2 receptor gene is associated with emotional control as well as brain activity and connectivity during emotion processing in humans. *J. Neurosci.* **29**, 14812–14819.

Boutz P., Stoilov P., Li Q. *et al.* (2007) A post-transcriptional regulatory switch in polypyrimidine tract-binding proteins reprograms alternative splicing in developing neurons. *Genes Dev.* **21**, 1636–1652.

Centonze D., Usiello A., Gubellini P., Pisani A., Borrelli E., Bernardi G. and Calabresi P. (2002) Dopamine D2 receptor-mediated inhibition of dopaminergic neurons in mice lacking D2L receptors. *Neuropsychopharmacology* **27**, 723–726.

Centonze D., Gubellini P., Usiello A. *et al.* (2004) Differential contribution of dopamine D2S and D2L receptors in the modulation of glutamate and GABA transmission in the striatum. *Neuroscience* **129**, 157–166.

Cooper T. A. (2005) Use of minigene systems to dissect alternative splicing elements. *Methods* **37**, 331–340.

Grossman J., Meyer M., Wang Y., Mulligan G., Kobayashi R. and Helfman D. (1998) The use of antibodies to the polypyrimidine tract binding protein (PTB) to analyze the protein components that assemble on alternatively spliced pre-mRNAs that use distant branch points. *RNA* **4**, 613–625.

Guiramand J., Montmayeur J., Ceraline J., Bhatia M. and Borrelli E. (1995) Alternative splicing of the dopamine D2 receptor directs specificity of coupling to G-proteins. *J. Biol. Chem.* **270**, 7354–7358.

Guivarc'h D., Vernier P. and Vincent J. (1995) Sex steroid hormones change the differential distribution of the isoforms of the D2 dopamine receptor messenger RNA in the rat brain. *Neuroscience* **69**, 159–166.

Guivarc'h D., Vincent J. and Vernier P. (1998) Alternative splicing of the D2 dopamine receptor messenger ribonucleic acid is modulated by activated sex steroid receptors in the MMQ prolactin cell line. *Endocrinology* **139**, 4213–4221.

Hranilovic D., Bucan M. and Wang Y. (2008) Emotional response in dopamine D2L receptor-deficient mice. *Behav. Brain Res.* **195**, 246–250.

Khan Z., Mrzljak L., Gutierrez A., de la Calle A. and Goldman-Rakic P. (1998) Prominence of the dopamine D2 short isoform in dopaminergic pathways. *Proc. Natl Acad. Sci. USA* **95**, 7731–7736.

Kino Y., Washizu C., Oma Y., Onishi H., Nezu Y., Sasagawa N., Nukina N. and Ishiura S. (2009) MBNL and CELF proteins regulate alternative splicing of the skeletal muscle chloride channel CLCN1. *Nucleic Acids Res.* **37**, 6477–6490.

Knoch K., Meisterfeld R., Kersting S., Bergert H., Altkrüger A., Wegbrod C., Jäger M., Saeger H. and Solimena M. (2006) cAMP-dependent phosphorylation of PTB1 promotes the expression of insulin secretory granule proteins in beta cells. *Cell Metab.* **3**, 123–134.

Li Q., Lee J. and Black D. (2007) Neuronal regulation of alternative pre-mRNA splicing. *Nat. Rev. Neurosci.* **8**, 819–831.

Lindgren N., Usiello A., Goiny M., Haycock J., Erbs E., Greengard P., Hokfelt T., Borrelli E. and Fisone G. (2003) Distinct roles of dopamine D2L and D2S receptor isoforms in the regulation of protein phosphorylation at presynaptic and postsynaptic sites. *Proc. Natl Acad. Sci. USA* **100**, 4305–4309.

Makeyev E., Zhang J., Carrasco M. and Maniatis T. (2007) The micrRNA miR-124 promotes neuronal differentiation by triggering brain-specific alternative pre-mRNA splicing. *Mol. Cell* **27**, 435–448.

Oomizu S., Boyadjieva N. and Sarkar D. (2003) Ethanol and estradiol modulate alternative splicing of dopamine D2 receptor messenger RNA and abolish the inhibitory action of bromocriptine on prolactin release from the pituitary gland. *Alcohol. Clin. Exp. Res.* **27**, 975–980.

Senogles S. (1994) The D2 dopamine receptor isoforms signal through distinct Gi alpha proteins to inhibit adenylyl cyclase. A study with site-directed mutant Gi alpha proteins. *J. Biol. Chem.* **269**, 23120–23127.

Senogles S., Heimert T., Odife E. and Quasney M. (2004) A region of the third intracellular loop of the short form of the D2 dopamine receptor dictates Gi coupling specificity. *J. Biol. Chem.* **279**, 1601–1606.

Sharma S., Kohlstaedt L., Damianov A., Rio D. and Black D. (2008) Polypyrimidine tract binding protein controls the transition from exon definition to an intron defined spliceosome. *Nat. Struct. Mol. Biol.* **15**, 183–191.

Usiello A., Baik J., Rougé-Pont F., Picetti R., Dierich A., LeMeur M., Piazza P. and Borrelli E. (2000) Distinct functions of the two isoforms of dopamine D2 receptors. *Nature* **408**, 199–203.

Wagner E. and Garcia-Blanco M. (2001) Polypyrimidine tract binding protein antagonizes exon definition. *Mol. Cell. Biol.* **21**, 3281–3288.

Wang Y., Xu R., Sasaoka T., Tonegawa S., Kung M. and Sankoorikal E. (2000) Dopamine D2 long receptor-deficient mice display alterations in striatum-dependent functions. *J. Neurosci.* **20**, 8305–8314.

Xie J., Lee J., Kress T., Mowry K. and Black D. (2003) Protein kinase A phosphorylation modulates transport of the polypyrimidine tract-binding protein. *Proc. Natl Acad. Sci. USA* **100**, 8776–8781.

Zhang Y., Bertolino A., Fazio L. *et al.* (2007) Polymorphisms in human dopamine D2 receptor gene affect gene expression, splicing, and neuronal activity during working memory. *Proc. Natl Acad. Sci. USA* **104**, 20552–20557.

THE JOURNAL OF BIOLOGICAL CHEMISTRY VOL. 285, NO. 3, pp. 1634–1642, January 15, 2010

β-Secretase Inhibitor Potency Is Decreased by Aberrant β-Cleavage Location of the "Swedish Mutant" Amyloid Precursor Protein

Received for publication, September 21, 2009, and in revised form, November 16, 2009 Published, JBC Papers in Press, November 19, 2009, DOI 10.1074/jbc.M109.066753

Hidekuni Yamakawa, Sosuke Yagishita, Eugene Futai, and Shoichi Ishiura[1]

From the Department of Life Sciences, Graduate School of Arts and Sciences, University of Tokyo, Meguro-ku, Tokyo 153-8902, Japan

The amyloid-β (Aβ) peptide, widely known as the causative molecule of Alzheimer disease (AD), is generated by the sequential cleavage of amyloid precursor protein (APP) by the aspartyl proteases BACE1/β-secretase and presenilin/γ-secretase. Inhibition of BACE1, therefore, is a promising strategy for preventing the progression of AD. However, β-secretase inhibitors (BSIs) exhibit unexpectedly low potency in cells expressing "Swedish mutant" APP (APPswe) and in the transgenic mouse Tg2576, an AD model overexpressing APPswe. The Swedish mutation dramatically accelerates β-cleavage of APP and hence the generation of Aβ; this acceleration has been assumed to underlie the poor inhibitory activity of BSI against APPswe processing. Here, we studied the mechanism by which the Swedish mutation causes this BSI potency decrease. Surprisingly, decreased BSI potency was not observed in an *in vitro* assay using purified BACE1 and substrates, indicating that the accelerated β-cleavage resulting from the Swedish mutation is not its underlying cause. By focusing on differences between the cell-based and *in vitro* assays, we have demonstrated here that the potency decrease is caused by the aberrant subcellular localization of APPswe processing and not by accelerated β-cleavage or the accumulation of the C-terminal fragment of β-cleaved APP. Because most patients with sporadic AD express wild type APP, our findings suggest that the wild type mouse is superior to the Tg2576 mouse as a model for determining the effective dose of BSI for AD patients. This work provides novel insights into the potency decrease of BSI and valuable suggestions for its development as a disease-modifying agent.

Alzheimer disease (AD)[2] is the most common type of dementia associated with neurodegeneration. Amyloid β (Aβ) peptides accumulate in the brains of AD patients and are deposited as insoluble plaques, the hallmarks of AD pathophysiology (1). Aβ is produced by sequential cleavage of amyloid precursor protein (APP) by the aspartyl proteases BACE1/β-secretase and presenilin/γ-secretase. Growing evidence indicates that the acceleration of Aβ generation can trigger the cognitive dysfunction characteristic of AD (2–4). In fact, many risk factors for AD, including higher levels of β-secretase and γ-secretase expression, oxidative stress, and insulin dysfunction, promote the generation of Aβ (5–11). Therefore, the inhibition of Aβ production is one of the most promising therapeutic approaches for preventing the progression of AD (12–16).

BACE1/β-secretase inhibitors (BSIs) have been investigated as AD-modifying agents since the gene encoding the BACE1 enzyme was cloned in 1999 (17, 18). BACE1-deficient mice are viable, and the dramatic decrease in Aβ levels caused by the genetic deletion of BACE1 in AD model mice can ameliorate AD phenotypes such as memory impairment (19–21). However, BSI is less able to reduce Aβ in an AD model mouse (Tg2576) than in wild type mice (22–24), raising doubts about the potential clinically effective dose of BSI and thus raising concerns about the safety of the treatment and its cost in clinical trials.

Tg2576 is a transgenic mouse expressing "Swedish mutant" APP (APPswe) (25). This two-amino acid mutation, which was discovered in Swedish familial AD patients (26), dramatically accelerates β-site processing of APP. Therefore, the weakening of BSI potency in the Tg2576 mouse appears to be attributable to the Swedish mutation. Several reports have shown that BSIs are less potent against Aβ generation in cells stably transfected with the APPswe variant than in those transfected with wild type APP (APPwt) (22–24, 27), but the mechanism underlying this reduction in BSI inhibitory activity has not yet been elucidated. If the poor potency of BSIs in Tg2576 mice arises from differences between AD and non-AD that are unrelated to the Swedish mutation, then a high dose of BSI would be required to effectively prevent AD progression in both sporadic and Swedish type AD. Therefore, to accurately predict the clinically effective dose of BSI, we must elucidate the mechanism by which the Swedish mutation affects BSI potency.

In this study, *in vitro* BSI assays using purified BACE1 and substrate peptides showed that, in contrast to previous results from cell-based assays, BSI is as potent a cleavage inhibitor for APPswe as it is for APPwt. This finding suggests that differences between the cell-based and *in vitro* enzymatic assays might underlie the apparent effect of the Swedish mutation on BSI potency. Our analysis of these differences demonstrates that the potency decrease is caused by the aberrant subcellular localization of APPswe processing and not by accelerated β-cleavage or by the accumulation of the C-terminal fragment

[1] To whom correspondence should be addressed: 3-8-1 Komaba, Meguro-ku, Tokyo 153-8902, Japan. Tel. and Fax: 81-3-5454-6739; E-mail: cishiura@mail.ecc.u-tokyo.ac.jp.

[2] The abbreviations used are: AD, Alzheimer disease; APP, amyloid precursor protein; BSI, β-secretase inhibitor; βCTF, C-terminal fragment of β-cleaved APP; TBS, Tris-buffered saline; wt, wild type; Swe, Swedish type; SHwt, SH-SY5Y stably expressing APPwt; SHswe, SH-SY5Y stably expressing APPswe; Aβ, amyloid β; DMSO, dimethyl sulfoxide; BSA, bovine serum albumin; ELISA, enzyme-linked immunosorbent assay; HBSS, Hanks' balanced salt solution; PBS, phosphate-buffered saline; MES, 4-morpholineethanesulfonic acid.

of β-cleaved APP (βCTF). Our findings suggest that the abnormal subcellular site of APPswe processing is responsible for the weakened inhibitory activity of BSIs against Aβ production in APPswe-expressing cells.

EXPERIMENTAL PROCEDURES

In Vitro BACE1 Activity Assay—*In vitro* BACE1 activity assays were performed using substrate peptides from the American Peptide Company, Inc. (Sunnyvale, CA), recombinant human BACE1 from R & D Systems (Minneapolis, MN), and BSI OM99-2 (28) or β-secretase Inhibitor IV from Calbiochem (29). The substrate peptide sequences were SEVKMDAEFRHDSGYEK-biotin (wild type; wt) and SEVNLDAEFRHDSGYEK-biotin (Swedish; swe). Peptides and inhibitors were dissolved in dimethyl sulfoxide (DMSO), and dissolved peptides were stored at −20 °C.

The standard reaction buffer was 50 mM sodium acetate, pH 4.5, containing 0.25 mg/ml bovine serum albumin (BSA). In experiments to check the pH dependence of IC_{50} values, citrate-phosphate buffer was used because of its broad buffering range. The reactions were carried by mixing 89 μl of substrate solution, 1 μl of inhibitor solution or DMSO, and 10 μl of BACE1 in each well of a 96-well plate and incubating the plate under the conditions described in Fig. 1 and Table 1. The reactions were terminated by the addition of 30 μl of 1 M Tris-HCl, pH 7.6.

Enzyme-linked immunosorbent assays (ELISAs) were used to measure the products of BACE1 enzymatic cleavage. The reaction mixtures were appropriately diluted in Tris-buffered saline (TBS) containing 0.1% Tween 20 (TBST) and 1% BSA and transferred to a detection plate coated with a monoclonal antibody specific for the N-terminal end generated by BACE1 cleavage (82E1; IBL Co., Ltd., Gunma, Japan). The plate was incubated overnight at 4 °C and then washed five times with TBST. Neutravidin-horseradish peroxidase (Thermo Scientific, Inc., Rockford, IL) was diluted 1:10,000 in sample dilution buffer, and 100 μl of this diluted solution was added to each well. The plate was incubated for 1 h at room temperature, washed five times with TBST, and developed using SuperSignal ELISA Pico chemiluminescent substrate (Thermo Scientific, Inc.). Luminescence counts were measured using an ARVO MX plate reader (PerkinElmer Life Sciences).

Cell-based Aβ Production Activity Assay—SH-SY5Y human neuroblastoma cells stably transfected with APP isoform 695 (APP695) were maintained in Dulbecco's modified Eagle's medium containing 10% heat-inactivated fetal bovine serum (4.5 g/liter) and 100 μg/ml hygromycin B. Cells transfected with wild type or Swedish mutant APP695 (APPwt or APPswe, respectively) were designated SHwt cells and SHswe cells, respectively. For inhibitor treatments, the cells were seeded in 96-well plates at a density of 8×10^5 cells/ml (150 μl of growth medium/well), incubated for 2 h, and then treated with 2 μl of inhibitor diluted in DMSO. The final DMSO concentration was 1%. The cells were then incubated for 24 h at 37 °C in a humidified 5% CO_2 atmosphere. To measure secreted Aβ, the conditioned medium was transferred to a 96-well plate, which was stored at 4 °C until use.

For quantification of βCTF, treated cells were lysed in TBS containing Complete protease inhibitor mixture (Roche Applied Science) and 1% Triton X-100 for 2 h at 4 °C. The amount of βCTF in the lysate was determined using a βCTF ELISA.

Cell Surface Biotinylation—Five milliliters of SHwt or SHswe cells were seeded into 6-cm dishes (2×10^6 cells/dish). After 24 h, the cells were washed three times with Hanks' balanced salt solution (HBSS) and then biotinylated with Sulfo-NHS-LC-Biotin (0.5 mg/ml; Thermo Scientific, Inc.) in cold HBSS for 1 h at 4 °C. The cultures were washed with 100 mM glycine in cold HBSS and rinsed twice with cold HBSS. The cells were harvested in cold phosphate-buffered saline (PBS) and collected by centrifugation. Cell pellets were suspended in PBS containing 1% Nonidet P-40 and Complete protease inhibitor mixture (Roche Applied Science), sonicated, and centrifuged at 16,000 × *g* for 10 min. The protein concentrations of the supernatant fractions were determined using a BCA assay kit (Thermo Scientific, Inc.) and normalized to the controls.

The normalized SHwt and SHswe cell lysates were incubated with streptavidin beads (Thermo Scientific, Inc.) overnight. The biotinylated molecules were eluted by heating at 95 °C for 10 min in LDS sample buffer (Invitrogen). The eluates were analyzed by Western blotting using anti-APP antibody 6E10 (Covance, Princeton, NJ).

Immunofluorescence and Image Acquisition—SHwt or SHswe cells cultured on plastic discs in 24-well plates were rinsed with HBSS, incubated with antibody 6E10 (1:200) to label APP on the cell surface, and washed three times with cold HBSS. Either immediately thereafter or after a 15-min incubation at 37 °C to allow endocytosis to occur, the cells were fixed for 15 min at room temperature in 4% paraformaldehyde. The fixed cells were permeabilized, blocked with PBS containing 0.1% Triton X-100 and 3% normal goat serum for 15 min, and incubated with a rabbit polyclonal antibody specific for the C-terminal region of APP (AB5352; Millipore, Billerica, MA) overnight at 4 °C. The primary antibodies were labeled with secondary antibodies conjugated to Alexa Fluor 488 (for AB5352) or 594 (for 6E10) (Invitrogen). The images were acquired using an Eclipse FN1 microscope (Nikon, Tokyo, Japan) equipped with a 40× objective. Exposure time and gain remained constant for all of the images.

Cell-free β-Secretase Assay—SHwt and SHswe cell lysates were assayed for β-secretase in a cell-free system. First, SHwt and SHswe cells were cultured in 150-mm dishes, washed with PBS, suspended with trypsin-EDTA, diluted with growth medium, and centrifuged. The resulting cell pellets were washed twice with PBS and quickly frozen in liquid N_2. Frozen cells were homogenized in a buffer containing 50 mM MES, pH 5.5, Complete protease inhibitor mixture (Roche Applied Science), the aspartic protease inhibitor pepstatin A (10 μM; Roche Applied Science), and the γ-secretase inhibitor *N*-[*N*-(3,5-difluorophenacetyl-L-alanyl)]-*S*-phenylglycine *t*-butyl ester (10 μM; Calbiochem) using 30 strokes of a tight fitting Dounce homogenizer. The lysis buffer was detergent-free to avoid disruption of the conformation of the APP substrate and BACE1 enzyme.

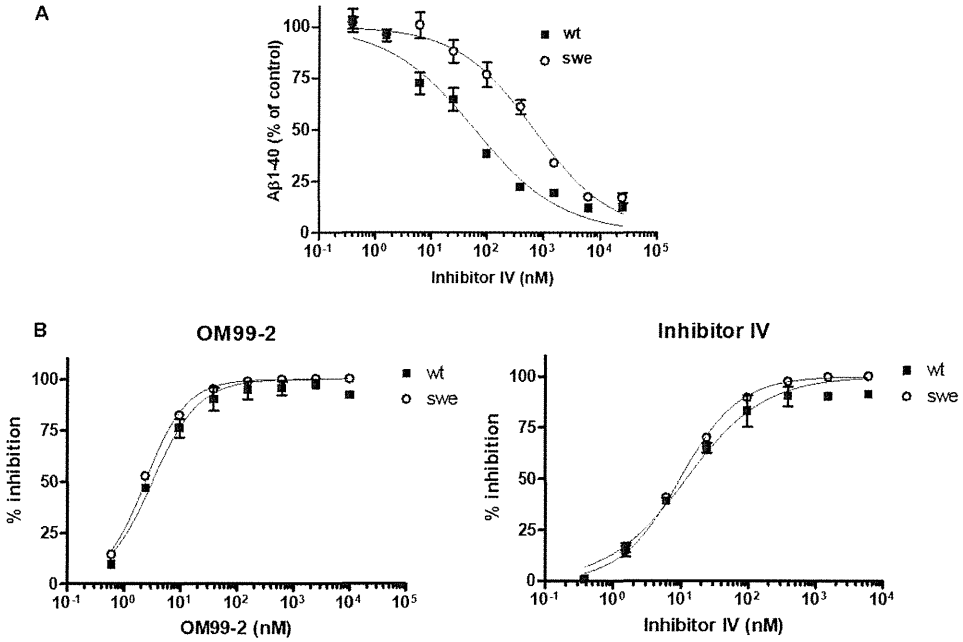

FIGURE 1. **The β-cleavage of wild type and "Swedish mutant" APP substrates is inhibited with equal efficiency by BSIs in an *in vitro* BACE1 activity assay.** *A*, SH-SY5Y cells stably transfected with wild type APP (APPwt; ■) or "Swedish mutant" APP (APPswe; ○) were treated with Inhibitor IV at the indicated concentrations for 24 h, and the conditioned medium was analyzed for the amount of $A\beta_{1-40}$ as described under "Experimental Procedures." $A\beta_{1-40}$ quantification data are expressed relative to those for DMSO-treated control cultures (defined as 100%). The IC_{50} values for APPwt and APPswe are 61 and 694 nM, respectively. *B*, an *in vitro* BACE1 assay was performed using 0.45 nM purified human BACE1, 4 μM substrate peptide (a greater than 100-fold excess of substrate), and the indicated concentrations of BSI OM99-2 or Inhibitor IV. The inhibition data are expressed relative to control reaction mixtures lacking BACE1 enzyme (defined as 100%). However, 0% inhibition is defined as that obtained for a control solution treated with DMSO (no inhibitor).

TABLE 1

Summary of IC_{50} values for BSIs in an in vitro BACE1 assay under various conditions

Parameter	IC_{50} ± S.D.		IC_{50} ratio (swe:wt)
	Wt	Swe	
	nm		
β-Secretase inhibitor compound			
OM99-2	3.3 ± 0.3	2.4 ± 0.1	0.7
Inhibitor IV	12.4 ± 2.3	9.8 ± 0.9	0.8
Reaction time[a]			
3 h	3.5 ± 0.5	4.1 ± 1.0	1.2
6 h	5.4 ± 1.9	8.2 ± 1.4	1.5
24 h	6.0 ± 1.1	9.4 ± 0.5	1.5
Substrate/enzyme ratio[a]			
200:1	19 ± 2	23 ± 6	1.2
50:4	21 ± 3	28 ± 6	1.3
25:8	24 ± 5	32 ± 6	1.4
16:16	26 ± 6	46 ± 10	1.7
pH[a]			
4.6	5.6 ± 1.0	5.0 ± 1.1	0.9
6.2	5.6 ± 0.4	4.6 ± 1.7	0.8

[a] These experiments were performed using Inhibitor IV.

The cell lysates were mixed in 96-well plates with reaction buffer containing various concentrations of Inhibitor IV and incubated for 1 h at 25 °C with shaking. The reactions were terminated by the addition of 1 M Tris-HCl, pH 7.6, containing 3% Triton X-100 and 50 μM Inhibitor IV. Solubilized βCTF was quantified using an ELISA.

Quantification of $A\beta_{1-40}$, $A\beta_{1-x}$, and βCTF—An $A\beta_{1-40}$ homogenous time resolved fluoresence kit was purchased from Nihon Schering (Osaka, Japan). Briefly, antibody-EuK (55 ng/ml), antibody-XL665 (400 ng/ml), and phosphate buffer (50 mM; pH 7.4) containing 0.2% BSA and 0.5 M KF were added into each well of a 384-well plate. Samples of conditioned cell culture medium or synthetic peptide standards were added to yield a total assay volume of 20 μl/well. After mixing, the reaction mixture was incubated at 4 °C to reach equilibrium binding and then read on an ARVO multilabel counter (PerkinElmer Life Sciences).

An $A\beta_{1-x}$ ELISA was established using the commercially available antibodies 82E1 (IBL Co., Ltd.) and 4G8 (Covance). First, a Maxisorp plate (Nunc, Rochester, NY) was coated with 82E1 (0.5 μg/ml) in 50 mM Tris-HCl, pH 8, overnight at 4 °C and then blocked with TBST containing 0.5% BSA. Next, conditioned medium was appropriately diluted with sample dilution buffer (TBST containing 1% BSA), added to the 82E1-coated wells, and incubated overnight at 4 °C. After four washes, horseradish peroxidase-conjugated 4G8 (0.05 μg/ml in sample dilution buffer) was added, and the mixture was incubated for 1 h at room temperature. The peptides sandwiched with both 82E1 and 4G8 were quantified as luminescence counts (see "*In Vitro* BACE1 Activity Assay"). βCTF was quantified using a βCTF ELISA kit (IBL Co., Ltd.) according to the manufacturer's protocol.

Data Analysis—GraphPad Prism (GraphPad Software, Inc., San Diego, CA) was used to graph and analyze data. All of the titration curves were fitted to a sigmoidal dose-response equation to determine the IC_{50} values of the tested compounds.

RESULTS

BSIs Are Equally Potent Inhibitors of BACE1 Cleavage of APPwt and APPswe in Vitro—It has been widely observed that, in cells, BSIs are much less effective inhibitors of β-cleavage of APPswe than of β-cleavage of APPwt (22–24, 27). In the present study, we assessed the relative effectiveness of Inhibitor IV at reducing the production of Aβ in SH-SY5Y cells stably expressing APPwt *versus* APPswe. As shown in Fig. 1*A*, Inhibitor IV was about 10-fold less potent against β-cleavage of APPswe in SH-SY5Y cells than against the β-cleavage of APPwt reported previously.

The Swedish mutation dramatically accelerates β-cleavage of APP in both *in vitro* enzymatic assays and in cell-based assays. Therefore, we investigated whether it would cause a similar decrease in BSI potency *in vitro* using purified BACE1 and substrate peptides. The IC_{50} values of inhibitors of BACE1 activity are summarized in Table 1. The representative BACE1 inhibitors OM99-2 and Inhibitor IV were

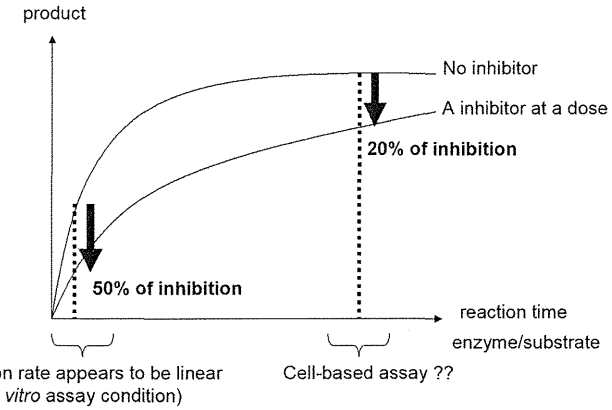

FIGURE 2. **Schematic model of the "saturation hypothesis."** In this hypothetical scheme, inhibitors are less powerful under product-saturated conditions arising from lengthy reaction times or an excessively high enzyme: substrate ratio.

equally potent inhibitors of cleavage of the wild type and Swedish type substrates.

The APPswe-induced Decrease in BSI Potency Observed in Cells Does Not Occur in Vitro under Various Cell-like Conditions—The discrepancy between *in vitro* and cell-based assay data suggests that the decreased potency of BSI in cells expressing APPswe might result from differences between the two assays. Not only do the assays differ in reaction conditions, such as the enzyme: substrate ratio, reaction time, and pH, but they also differ in that βCTF accumulates in cells expressing APPswe and in the subcellular compartmentalization of the β-cleavage reaction.

We first examined the influence of reaction conditions on the IC_{50} value of BSI. Generally, an enzymatic reaction proceeds linearly during the early phase and then reaches a plateau; the percentage of inhibition generally appears to be lower at the plateau than in the early phase (Fig. 2). Because cell-based assays usually use longer reaction times than those *in vitro*, the BACE1 cleavage reaction might be saturated under cell-based assay conditions. In addition, because the k_{cat}/K_m of APPswe is much higher than that of APPwt, the β-cleavage reaction may reach a plateau much earlier for APPswe than for APPwt. We speculated that in cells, the saturation of BACE1 cleavage of APPswe might decrease the potency of BSI. Therefore, we performed *in vitro* BACE1 activity assays for various lengths of time and compared the resulting IC_{50} values for the processing of the Swedish and wild type peptides. Unexpectedly, the ratio of IC_{50} values for APPswe and APPwt (IC_{50} swe:wt) did not increase with longer reaction times (Table 1). Even after 24 h, the IC_{50} value of swe:wt was much less than 10, and it was the same as that in the cell-based assay.

Next, to examine the saturation hypothesis (see the schematic in Fig. 2), we incubated BACE1:substrate mixtures of various ratios for 24 h to bring the reactions closer to plateau. Even when BACE1 and its substrate were present in equal amounts, IC_{50} swe:wt was still much less than 10 (Table 1), which is inconsistent with the saturation hypothesis.

We next examined whether pH conditions might affect BSI potency. Although APP was previously thought to be cleaved by BACE1 in acidic cell compartments of pH 4.5, the optimal pH for BACE1, β-cleavage of APP occurs in early endosomes with a

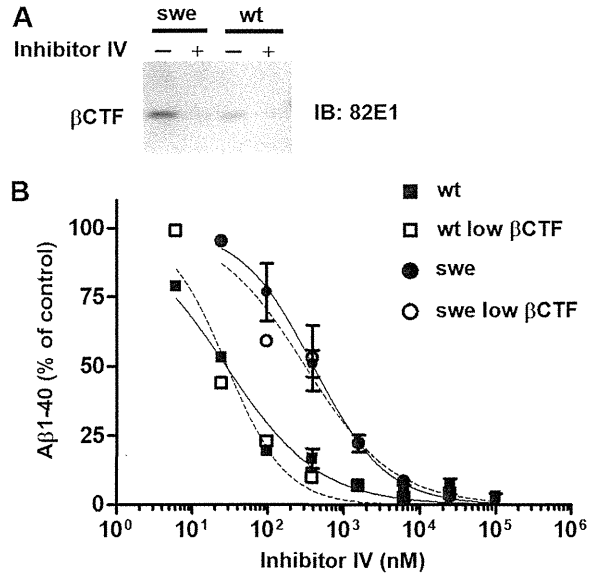

FIGURE 3. **βCTF accumulation is not the cause of the Swedish mutation-linked reduction in BSI Aβ-reducing potency in APPswe-expressing SH-SY5Y cells.** *A*, Western blot demonstrating robust accumulation of C-terminal fragments of β-cleaved APP (βCTF) in SH-SY5Y cells stably transfected with APPswe (SHswe cells) but not in SH-SY5Y cells stably expressing APPwt (SHwt cells). Pretreatment with Inhibitor IV (25 μM) for 24 h reduced the level of βCTF in pretreated SHswe cells to a level below that in SHwt cells pretreated with DMSO. *B*, SHwt and SHswe cells pretreated with Inhibitor IV or DMSO were treated again with Inhibitor IV at the indicated concentrations for 24 h, and the amount of $A\beta_{1-40}$ in the conditioned medium was measured as described under "Experimental Procedures." The data for $A\beta_{1-40}$ levels in the culture medium are expressed relative to the data for medium from DMSO-treated control cultures (defined as 100%). The IC_{50} values with and without pretreatment were as follows: SHwt, 28 nM; pretreated SHwt (low βCTF), 29 nM; SHswe, 400 nM; pretreated SHswe (low βCTF), 311 nM. *IB*, immunoblot.

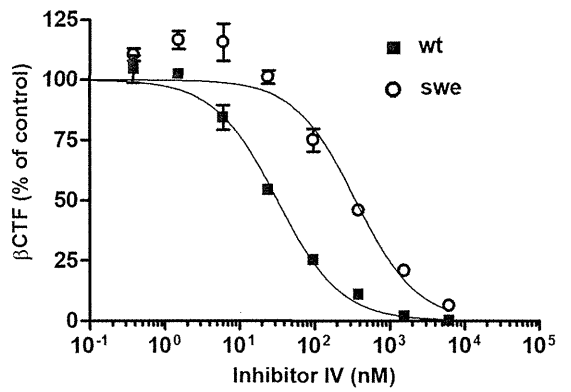

FIGURE 4. **BSI inhibits the generation of βCTF in SH-SY5Y cells stably expressing Swedish type APP (SHswe) less potently than in SH-SY5Y cells stably expressing wild type APP (SHwt).** SHwt and SHswe cells were treated with Inhibitor IV at the indicated concentrations for 24 h and then lysed in Tris-buffered saline containing 1% Triton X-100. The amount of βCTF in the cell lysate was measured using a βCTF enzyme-linked immunosorbent assay kit (ELISA). The βCTF quantification data are expressed relative to those for the DMSO-treated control cultures (defined as 100%). The IC_{50} values in SHwt and SHswe cells are 32 and 356 nM, respectively.

pH of ~6 (30). We therefore examined whether the presence of a higher pH in the cellular compartments in which β-cleavage occurs might explain the decreased potency. We measured BACE1 activities at pH 4.5 and 6.2 and plotted the percentage of inhibition at each dose of Inhibitor IV (Table 1). Both the IC_{50} value and IC_{50} swe:wt remained unaffected by pH, indicating that the Swedish mutation-linked BSI potency decrease is not

caused by a higher pH in the cellular compartment in which β-cleavage of APP occurs.

βCTF Accumulation Is Not Involved in the BSI Potency Decrease—βCTF has been reported to accumulate robustly in cells stably expressing APPswe (22, 31), suggesting that the inhibition of βCTF production by BSI may not lower the amount of Aβ secreted from SHswe cells. Specifically, the βCTF that accumulates in SHswe cells can be cleaved by γ-secretase to release Aβ into the medium, which might then lead to the BSI potency decrease. In this case, inhibiting the accumulation of βCTF before assaying the BSI assay would abolish the apparent potency decrease. To examine this possibility, we performed cell-based assays with Inhibitor IV pretreatment to prevent the accumulation of βCTF. After 24 h of pretreatment (Fig. 3*A*), we exposed SHwt and SHswe cells to a range of Inhibitor IV concentrations and quantified the $A\beta_{1-40}$ secreted into the media. As shown in Fig. 3, the IC_{50} values for SHswe cells were about 10 times higher than those for SHwt cells, regardless of pretreatment conditions, indicating that βCTF accumulation in SHswe cells is not the cause of the reduced potency of BSI.

The Swedish Mutation Decreases BSI Potency against βCTF Production in a Cell-based Assay—To confirm that the reduced effectiveness of BSIs against APPswe processing is independent of βCTF accumulation, we investigated whether Inhibitor IV equally prevents βCTF generation in SHwt and SHswe cells. βCTF was quantified using a βCTF ELISA kit after the cells were exposed to various Inhibitor IV concentrations for 24 h. As shown in Fig. 4, Inhibitor IV exhibited the usual decrease in inhibitory activity in these experiments. In addition, the IC_{50} values for βCTF production were comparable with those for Aβ production. These data suggest that no association exists between the accumulation of βCTF and the decreased effectiveness of BSI.

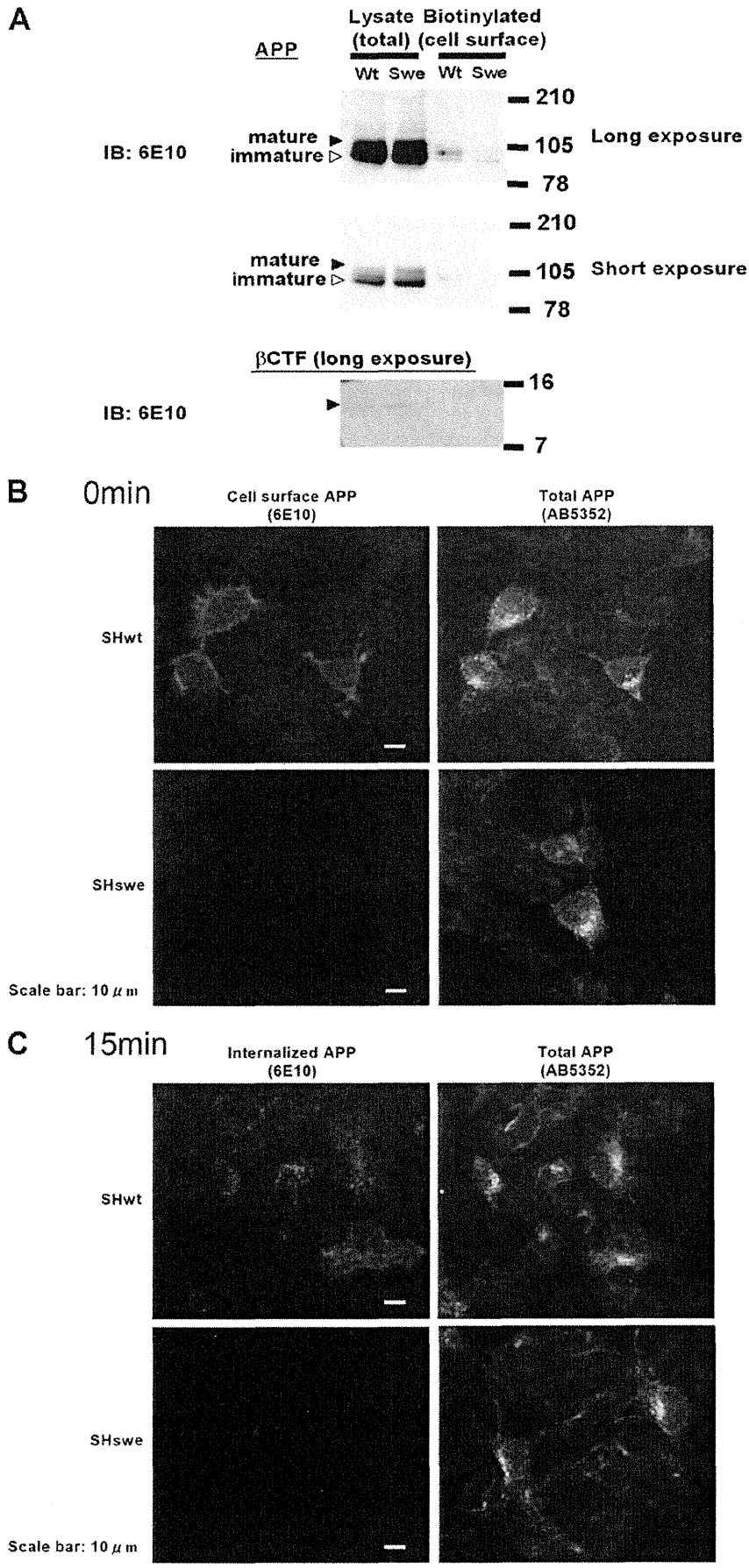

The Swedish Type APP Was Not Exposed to the Plasma Membrane, whereas Wild Type Was—The aberrant subcellular localization of APPswe processing by BACE1 has been reported by several groups (31, 34, 35, 40) with the specific consensus that although APPwt is cleaved by BACE1 in the early endosomes, the β-cleavage of APPswe occurs primarily within the secretory pathway. However, few studies have directly compared the localization of BACE1 processing for APPwt *versus* APPswe, particularly in human neuronal cells. Therefore, to confirm that the subcellular localization of APP processing by BACE1 is altered by the Swedish mutation, we compared the amounts of APPwt and APPswe reaching the plasma membrane without first undergoing β-cleavage in the secretory vesicles.

First, we labeled cell surface APP with biotin, precipitated the biotin-labeled APP using streptavidin beads, and quantified the biotin-labeled and total APP by Western blotting. As shown in Fig. 5*A*, the level of total APP in SHswe cells was similar to or higher than that in SHwt cells. In contrast, the level of biotin-labeled APP in SHswe cells was much lower than that in SHwt cells. In particular, mature, post-translationally modified APP was only minimally biotinylated in SHswe cells, suggesting that mature APPswe ready for processing by proteases is almost entirely cleaved by BACE1 before it appears on the cell surface.

Second, to demonstrate that most APPswe is neither exposed to the cell surface nor internalized by endocytosis, we conducted an immuno-uptake assay. APP on the SHwt and SHswe cell surfaces was labeled with the anti-APP antibody 6E10 and traced during its uptake by endocytosis. Although antibody 6E10 recognizes βCTF in addition to APP, the amount of βCTF was so much lower than that of APP (Fig. 5*A*) that we concluded that the observed 6E10 immunoreactivity was attributable to APP. As shown in Fig. 5*B*, the surfaces of SHwt cells, but not of SHswe cells, were substantially stained with 6E10. After a 15-min incubation at 37 °C to promote endocytosis, APP-bound 6E10 produced a fine granular staining pattern in SHwt cells but not in SHswe cells (Fig. 5*C*). In contrast, the anti-APP antibody AB5352 yielded comparable staining of total APP in SHwt and SHswe cells (Fig. 5, *B* and *C*, *right panels*). Taken together, these results indicate that APPswe does not reach the plasma membrane and is not endocytosed, unlike APPwt, suggesting that APPswe is mostly β-cleaved before it reaches the plasma membrane, whereas APPwt is β-cleaved after it reaches the plasma membrane.

BSI Equally Inhibits the Processing of APPwt and APPswe in a Cell-free Assay—Finally, we evaluated whether the subcellular compartment in which APP processing occurs influences the potency of BSI. Although APPwt is predominantly cleaved in early endosomes by BACE1 (32), the processing of APPswe occurs within the secretory pathway (33). Therefore, we investigated whether the distinct subcellular localization of β-cleavage leads to differences in the APPwt and APPswe processing

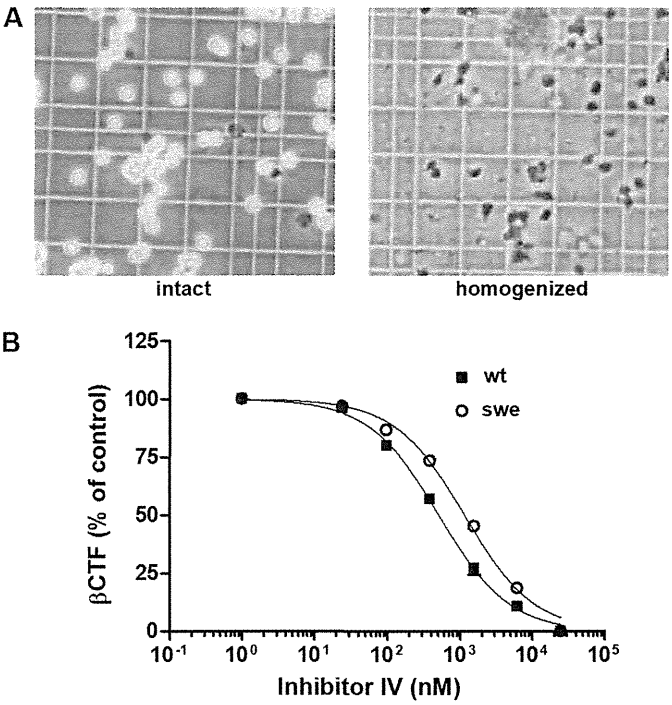

FIGURE 6. **In a cell-free assay with disrupted subcellular compartmentalization, BSI inhibits the processing of APPswe as effectively as APPwt.** *A*, intact or homogenized cells were suspended in phosphate-buffered saline containing 10% trypan blue and visualized under a microscope at 40× magnification. *B*, cells homogenized as in *A* were treated with Inhibitor IV at the indicated concentrations for 1 h at 25 °C, and the membranes were disrupted with 1% Triton X-100 to solubilize membrane-anchored βCTF. βCTF levels were determined using an ELISA; the βCTF quantification data are expressed relative to those for DMSO-treated control cell lysates (defined as 100%). The IC_{50} values for APPwt and APPswe are 514 and 1158 nM, respectively.

inhibition by BSI. In our cell-free assay, cellular compartments were thoroughly disrupted by homogenization, osmotic shock, and a freeze-thaw process (Fig. 6*A*). The resulting lysates were prepared in detergent-free lysis buffer to maintain protein conformations and protein-protein interactions. The SHwt and SHswe cell lysates were incubated in reaction buffer containing various concentrations of Inhibitor IV, and the percentage of inhibition by BSI relative to the DMSO control was plotted (Fig. 6*B*). Under these conditions, the IC_{50} values for APPswe and APPwt processing were comparable, suggesting that cellular partitioning is involved in the BSI potency decrease caused by the Swedish mutation.

In a Cell-based Assay, the Y687A Mutation Suppresses the Negative Effect of the Swedish Mutation on the Potency of BSI—The results of our cell-free assay suggested that the inhibitory potency of BSI depends on the subcellular location of APP β-cleavage. We therefore expected that restricting the subcellular site of β-cleavage would abolish the influence of the Swedish mutation on BSI potency. The trafficking and metabolism of APP is known to be regulated by its C-terminal region, which has the amino acid sequence YENPTY (34–38). Phosphoryla-

FIGURE 5. **The Swedish type APP is not exposed to the plasma membrane, whereas wild type is.** *A*, SHwt and SHswe cell surfaces were biotinylated for 1 h at 4 °C, conditions under which no endocytosis occurs. The biotinylated cell surface APP was precipitated with streptavidin-coated beads, and the precipitated and total APP were subjected to Western blot analysis with anti-APP antibody 6E10. *Black arrowheads* indicate mature APP; *white arrowheads* indicate immature APP. βCTF was barely detectable in the SHswe lysate lane. *B*, APP on the surface of SHwt and SHswe cells was labeled with antibody 6E10 for 45 min at 4 °C. After washing, the cells were immediately fixed with 4% paraformaldehyde. *Scale bar*, 10 μm. *C*, same as *B*, except that the washed cells were incubated for 15 min at 37 °C before fixing with 4% paraformaldehyde. *Scale bar*, 10 μm. *IB*, immunoblot.

tion of the tyrosine residue at position 687 in the C-terminal domain is essential for the localization of APP on the plasma membrane. In fact, the Y687A mutation of APP695 dramatically reduces the amount of APP on the cell surface (38). Furthermore, although the Y687A and wild type peptides are cleaved equally well by the purified α-secretase TACE in a cell-free assay, Y687A is poorly processed by cell surface α-secretase in a cell-based assay (38). Thus, full-length Y687A APP does not reach the plasma membrane and is strictly confined to the secretory vesicles even after its maturation in the Golgi apparatus. On the other hand, another study reported that the amount of secreted Aβ was unaffected by the Y687A mutation (36), indicating that, unlike the nonamyloidogenic α-secretase-dependent cleavage of APP, the amyloidogenic cleavage of APP by β- and γ-secretases could occur without reaching the cell surface.

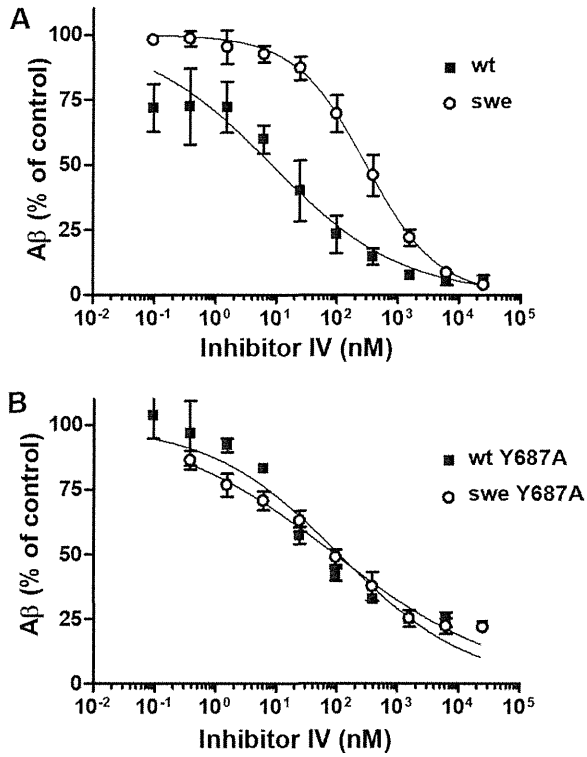

FIGURE 7. **BSI inhibits Aβ production in SH-SY5Y cells expressing the Y687A mutants of APPswe ($APPswe_{Y687A}$) and APPwt (APP_{Y687A}) with equal potency.** *A*, SHwt (■) and SHswe cells (○) were treated with Inhibitor IV at the indicated concentrations for 24 h, and the amount of Aβ in the conditioned medium was measured using an $Aβ_{1-x}$ ELISA. $Aβ_{1-x}$ quantification data are expressed relative to those for DMSO-treated control cultures (defined as 100%). The IC_{50} values for SHwt and SHswe are 19 and 298 nM, respectively. *B*, same as *A*, except that experiment was performed using SH-SY5Y cells stably expressing APP_{Y687A} (■) or $APPswe_{Y687A}$ mutants (○). The IC_{50} values for APP_{Y687A} and $APPswe_{Y687A}$ are 103 and 93 nM, respectively.

Hence, to clarify the mechanism by which the site of β-cleavage influences BSI potency, we inserted the Y687A mutation into APPwt and APPswe and analyzed the effect of Inhibitor IV on Aβ production in SH-SY5Y cells stably expressing these mutated proteins (APP_{Y687A} and $APPswe_{Y687A}$, respectively). Aβ production curves were produced by plotting the relative amount of $Aβ_{1-x}$ at each dose of Inhibitor IV. As shown in Fig. 7*B*, the curves for $APPswe_{Y687A}$ and APP_{Y687A} were nearly identical, whereas the fitted curve for APPswe was shifted to the right relative to that for APPwt (Fig. 7*A*). Thus, the ability of Inhibitor IV to prevent β-cleavage of Y687A-containing APP was independent of the β-cleavage site sequence, wild or Swedish type, supporting the hypothesis that the decreased effectiveness of BSI against APPswe cleavage is a result of differences in the subcellular sites of β-cleavage in APPwt- and APPswe-expressing cells.

DISCUSSION

Inhibition of β-secretase activity is the most promising strategy for modifying the course of AD, and many companies have long been attempting to develop BSIs for this purpose. To develop medicines with sufficient clinical efficacy, the preclinical data must allow accurate prediction of the clinically effective dose. Therefore, it is important to determine which of the model systems (wild type or Tg2576 mice) more accurately reflects AD patients in terms of the Aβ-lowering effectiveness of BSI and to elucidate the mechanism by which the Swedish mutation weakens the inhibitory potency of BSI.

We first attempted to recreate the BSI potency-decreasing effect of the Swedish mutant *in vitro* using purified BACE1 and substrates but were unable to adequately mimic cellular conditions. We then redirected our focus to a search for cellular conditions that would abolish the potency-decreasing effect of the Swedish mutant, *i.e.* we created a cell-based assay that was closer to *in vitro* conditions. By examining the ability of BSIs to reduce Aβ secretion from cells with no βCTF accumulation and their ability to inhibit the generation of βCTF, we unambiguously

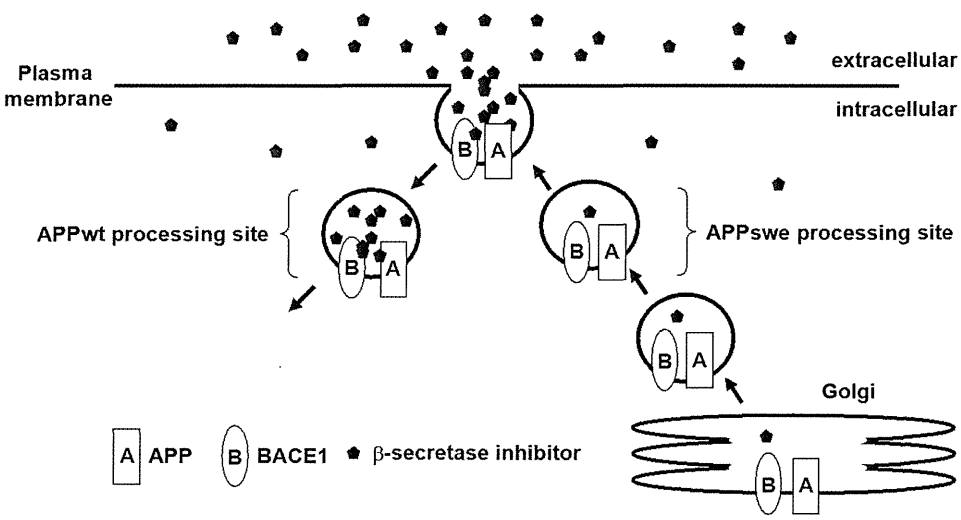

FIGURE 8. **Schematic diagram of the proposed model for increased BSI concentrations in early endosomes.** BSIs added to the medium are taken up by endocytosis and diffuse into compartments at various rates depending on their physical properties (such as cell permeability). Compounds bound to or adjacent to BACE1 on the cell surface are efficiently taken up into early endosomes, so that BSIs may be at higher concentrations in early endosomes than in secretory vesicles.

determined that βCTF accumulation does not underlie the potency-decreasing effect of the Swedish mutant, despite previous assertions to the contrary (22). Data from perturbation and alteration of the subcellular APP processing site suggest that the BSI potency decrease is, instead, a result of the anomalous subcellular localization of APPswe β-cleavage.

Why is the efficacy of BSI reduced by this change in the subcellular site of β-cleavage? Our findings give rise to two different speculations. First, the location of β-cleavage of APPswe might be generally difficult for chemicals to reach, probably because the place must be usually protected from exogenous enemies for cell survival. In fact, certain anti-cancer agents accumulate in certain organelles, thereby reducing their potency (39, 40), and Rajendran *et al.* (41) recently demonstrated that efficient targeting of BSI to the β-cleavage site can dramatically improve its inhibitory power against cellular Aβ production. These findings clearly indicate that drugs do not always spread into a cell uniformly and that their distribution patterns greatly influence their efficacies. Therefore, the notion that the BSI potency decrease is caused by a greatly decreased concentration of inhibitors at the subcellular site of APPswe β-cleavage is very reasonable. On the other hand, if this idea is indeed correct, then the potency decrease linked to the Swedish mutation would appear to be compound-specific rather than an example of a general phenomenon, considering that the distribution patterns of exogenous compounds are determined by particular physical characteristics. However, other groups have observed Swedish mutation-linked decreases in the potencies of several BSI series in cell-based assays (22, 24, 27). Moreover, we have confirmed that, in addition to Inhibitor IV, some compounds described in patents also exhibit the BSI potency decrease and that this decrease is abolished by the Y687A mutation (data not shown). These data suggest that most BSIs are distributed similarly in cells, probably because compounds with high affinities for the BACE1 active site share some physical properties.

A second, simpler explanation is that β-cleavage of APPswe occurs before it reaches the plasma membrane (31, 33), whereas APPwt is processed in an early endosome originating at the cell surface (32, 36). Both BACE1 and APP are transported from the Golgi apparatus to the plasma membrane and then to endosomes. The active site of BACE1 on the plasma membrane is exposed and more easily accessible to inhibitors than that of intracellular BACE1. BACE1 that cleaves APPwt is sometimes bound to BSI on the cell surface prior to APP processing, but the enzyme that processes APPswe is not. For either (or both) of the reasons described above (Fig. 8), the aberrant localization of APPswe processing may lower the potency of BSIs.

This work is important for the accurate estimation of clinically effective doses of BSIs. According to our results, the Aβ-lowering potency of BSI in sporadic AD patients may be better modeled by the wild type mouse than by the Tg2576 mouse. Almost all AD patients express wild type APP, suggesting that β-cleavage takes place during endocytosis, as in wild type mice. However, we cannot rule out the possibility that the location of APP processing is aberrant in sporadic AD patients, although no direct evidence supports this hypothesis. It has been reported that the trafficking and metabolism of APP are affected by the phosphorylation of its C terminus and by its interaction with X11, Fe65, LRP1, and others (10, 34, 42–47). Moreover, phosphorylation of APP has been observed in postmortem human brains (48). However, the pathophysiological role of APP phosphorylation remains controversial (49). In the near future, clinical data for BSI efficacy in AD patients, in combination with the results of this study, will enable us to infer the precise subcellular site of APP processing.

Acknowledgments—We thank all of the members of the Pain & Neurology Laboratory, particularly Dr. A. Kato, Dr. G. Sakaguchi, Dr. H. Ito, K. Nishitomi, A. Mikami, I. Nanchi, and M. Hosono (Shionogi & Co., Ltd.) for helpful discussions and technical suggestions.

REFERENCES

1. Selkoe, D. J., Bell, D. S., Podlisny, M. B., Price, D. L., and Cork, L. C. (1987) *Science* **235,** 873–877
2. Walsh, D. M., Klyubin, I., Fadeeva, J. V., Cullen, W. K., Anwyl, R., Wolfe, M. S., Rowan, M. J., and Selkoe, D. J. (2002) *Nature* **416,** 535–539
3. Klyubin, I., Walsh, D. M., Lemere, C. A., Cullen, W. K., Shankar, G. M., Betts, V., Spooner, E. T., Jiang, L., Anwyl, R., Selkoe, D. J., and Rowan, M. J. (2005) *Nat. Med.* **11,** 556–561
4. Shankar, G. M., Li, S., Mehta, T. H., Garcia-Munoz, A., Shepardson, N. E., Smith, I., Brett, F. M., Farrell, M. A., Rowan, M. J., Lemere, C. A., Regan, C. M., Walsh, D. M., Sabatini, B. L., and Selkoe, D. J. (2008) *Nat. Med.* **14,** 837–842
5. Yang, L. B., Lindholm, K., Yan, R., Citron, M., Xia, W., Yang, X. L., Beach, T., Sue, L., Wong, P., Price, D., Li, R., and Shen, Y. (2003) *Nat. Med.* **9,** 3–4
6. He, W., Lu, Y., Qahwash, I., Hu, X. Y., Chang, A., and Yan, R. (2004) *Nat. Med.* **10,** 959–965
7. Dodson, S. E., Gearing, M., Lippa, C. F., Montine, T. J., Levey, A. I., and Lah, J. J. (2006) *J. Neuropathol. Exp. Neurol.* **65,** 866–872
8. Harada, H., Tamaoka, A., Ishii, K., Shoji, S., Kametaka, S., Kametani, F., Saito, Y., and Murayama, S. (2006) *Neurosci. Res.* **54,** 24–29
9. Majercak, J., Ray, W. J., Espeseth, A., Simon, A., Shi, X. P., Wolffe, C., Getty, K., Marine, S., Stec, E., Ferrer, M., Strulovici, B., Bartz, S., Gates, A., Xu, M., Huang, Q., Ma, L., Shughrue, P., Burchard, J., Colussi, D., Pietrak, B., Kahana, J., Beher, D., Rosahl, T., Shearman, M., Hazuda, D., Sachs, A. B., Koblan, K. S., Seabrook, G. R., and Stone, D. J. (2006) *Proc. Natl. Acad. Sci. U.S.A.* **103,** 17967–17972
10. Ma, Q. L., Galasko, D. R., Ringman, J. M., Vinters, H. V., Edland, S. D., Pomakian, J., Ubeda, O. J., Rosario, E. R., Teter, B., Frautschy, S. A., and Cole, G. M. (2009) *Arch Neurol.* **66,** 448–457
11. Zhiyou, C., Yong, Y., Shanquan, S., Jun, Z., Liangguo, H., Ling, Y., and Jieying, L. (2009) *Neurochem. Res.* **34,** 1226–1235
12. Nishitomi, K., Sakaguchi, G., Horikoshi, Y., Gray, A. J., Maeda, M., Hirata-Fukae, C., Becker, A. G., Hosono, M., Sakaguchi, I., Minami, S. S., Nakajima, Y., Li, H. F., Takeyama, C., Kihara, T., Ota, A., Wong, P. C., Aisen, P. S., Kato, A., Kinoshita, N., and Matsuoka, Y. (2006) *J. Neurochem.* **99,** 1555–1563
13. Meredith, J. E., Jr., Thompson, L. A., Toyn, J. H., Marcin, L., Barten, D. M., Marcinkeviciene, J., Kopcho, L., Kim, Y., Lin, A., Guss, V., Burton, C., Iben, L., Polson, C., Cantone, J., Ford, M., Drexler, D., Fiedler, T., Lentz, K. A., Grace, J. E., Jr., Kolb, J., Corsa, J., Pierdomenico, M., Jones, K., Olson, R. E., Macor, J. E., and Albright, C. F. (2008) *J. Pharmacol. Exp. Ther.* **326,** 502–513
14. Sankaranarayanan, S., Price, E. A., Wu, G., Crouthamel, M. C., Shi, X. P., Tugusheva, K., Tyler, K. X., Kahana, J., Ellis, J., Jin, L., Steele, T., Stachel, S., Coburn, C., and Simon, A. J. (2008) *J. Pharmacol. Exp. Ther.* **324,** 957–969
15. Sankaranarayanan, S., Holahan, M. A., Colussi, D., Crouthamel, M. C., Devanarayan, V., Ellis, J., Espeseth, A., Gates, A. T., Graham, S. L., Gregro, A. R., Hazuda, D., Hochman, J. H., Holloway, K., Jin, L., Kahana, J., Lai, M. T., Lineberger, J., McGaughey, G., Moore, K. P., Nantermet, P., Pietrak, B., Price, E. A., Rajapakse, H., Stauffer, S., Steinbeiser, M. A., Seabrook, G., Selnick, H. G., Shi, X. P., Stanton, M. G., Swestock, J., Tugusheva, K., Tyler,

K. X., Vacca, J. P., Wong, J., Wu, G., Xu, M., Cook, J. J., and Simon, A. J. (2009) *J. Pharmacol. Exp. Ther.* **328,** 131–140
16. Asai, M., Hattori, C., Iwata, N., Saido, T. C., Sasagawa, N., Szabó, B., Hashimoto, Y., Maruyama, K., Tanuma, S., Kiso, Y., and Ishiura, S. (2006) *J. Neurochem.* **96,** 533–540
17. Sinha, S., Anderson, J. P., Barbour, R., Basi, G. S., Caccavello, R., Davis, D., Doan, M., Dovey, H. F., Frigon, N., Hong, J., Jacobson-Croak, K., Jewett, N., Keim, P., Knops, J., Lieberburg, I., Power, M., Tan, H., Tatsuno, G., Tung, J., Schenk, D., Seubert, P., Suomensaari, S. M., Wang, S., Walker, D., Zhao, J., McConlogue, L., and John, V. (1999) *Nature* **402,** 537–540
18. Vassar, R., Bennett, B. D., Babu-Khan, S., Kahn, S., Mendiaz, E. A., Denis, P., Teplow, D. B., Ross, S., Amarante, P., Loeloff, R., Luo, Y., Fisher, S., Fuller, J., Edenson, S., Lile, J., Jarosinski, M. A., Biere, A. L., Curran, E., Burgess, T., Louis, J. C., Collins, F., Treanor, J., Rogers, G., and Citron, M. (1999) *Science* **286,** 735–741
19. Ohno, M., Sametsky, E. A., Younkin, L. H., Oakley, H., Younkin, S. G., Citron, M., Vassar, R., and Disterhoft, J. F. (2004) *Neuron* **41,** 27–33
20. McConlogue, L., Buttini, M., Anderson, J. P., Brigham, E. F., Chen, K. S., Freedman, S. B., Games, D., Johnson-Wood, K., Lee, M., Zeller, M., Liu, W., Motter, R., and Sinha, S. (2007) *J. Biol. Chem.* **282,** 26326–26334
21. Ohno, M., Cole, S. L., Yasvoina, M., Zhao, J., Citron, M., Berry, R., Disterhoft, J. F., and Vassar, R. (2007) *Neurobiol. Dis.* **26,** 134–145
22. Riddell, D., Atchison, K., Yu, D., Turner, J., Wang, E., Gonzales, C., Warwick, H., Kim, J., Malamas, M., Wagner, E., Aschmies, S., Albinson, K., Erdel, J., Gunawan, I., Revilla-Sanchez, R., Takano, K., Warren, N., Fang, K., Bard, J., Hirst, W., Pangalos, M., Moss, S., Haydon, P., Robichaud, A., and Reinhart, P. (2009) in *International Conference on Alzheimer's Disease*, Vienna, Austria on July 15, 2009
23. Shitaka, Y., Yarimizu, J., Nagakura, A., Mitani, Y., TAkami, S., Miyake, A., Hamakawa, N., Hey, J., Koelsch, G., Bilcer, G., and Matsuoka, N. (2008) in *International Conference on Alzheimer's Disease*, Chicago, IL on July 28, 2008
24. Malamas, M., Erdei, J., Gunawan, I., Robichaud, A., Turner, J., Hu, Y., Wagner, E., Aschmies, S., Comery, T., and Fan, K. (2008) in *International Conference on Alzheimer's Disease,* Chicago, IL on July 28, 2008, **4,** 515–515
25. Hsiao, K., Chapman, P., Nilsen, S., Eckman, C., Harigaya, Y., Younkin, S., Yang, F., and Cole, G. (1996) *Science* **274,** 99–102
26. Citron, M., Oltersdorf, T., Haass, C., McConlogue, L., Hung, A. Y., Seubert, P., Vigo-Pelfrey, C., Lieberburg, I., and Selkoe, D. J. (1992) *Nature* **360,** 672–674
27. Hussain, I., Hawkins, J., Harrison, D., Hille, C., Wayne, G., Cutler, L., Buck, T., Walter, D., Demont, E., Howes, C., Naylor, A., Jeffrey, P., Gonzalez, M. I., Dingwall, C., Michel, A., Redshaw, S., and Davis, J. B. (2007) *J. Neurochem.* **100,** 802–809
28. Hong, L., Koelsch, G., Lin, X., Wu, S., Terzyan, S., Ghosh, A. K., Zhang, X. C., and Tang, J. (2000) *Science* **290,** 150–153
29. Pietrak, B. L., Crouthamel, M. C., Tugusheva, K., Lineberger, J. E., Xu, M., DiMuzio, J. M., Steele, T., Espeseth, A. S., Stachel, S. J., Coburn, C. A., Graham, S. L., Vacca, J. P., Shi, X. P., Simon, A. J., Hazuda, D. J., and Lai, M. T. (2005) *Anal. Biochem.* **342,** 144–151
30. Stachel, S. J., Coburn, C. A., Rush, D., Jones, K. L., Zhu, H., Rajapakse, H., Graham, S. L., Simon, A., Katharine Holloway, M., Allison, T. J., Munshi, S. K., Espeseth, A. S., Zuck, P., Colussi, D., Wolfe, A., Pietrak, B. L., Lai, M. T., and Vacca, J. P. (2009) *Bioorg Med. Chem. Lett.* **19,** 2977–2980
31. Thinakaran, G., Teplow, D. B., Siman, R., Greenberg, B., and Sisodia, S. S. (1996) *J. Biol. Chem.* **271,** 9390–9397
32. Koo, E. H., and Squazzo, S. L. (1994) *J. Biol. Chem.* **269,** 17386–17389
33. Haass, C., Lemere, C. A., Capell, A., Citron, M., Seubert, P., Schenk, D., Lannfelt, L., and Selkoe, D. J. (1995) *Nat. Med.* **1,** 1291–1296
34. King, G. D., Perez, R. G., Steinhilb, M. L., Gaut, J. R., and Turner, R. S. (2003) *Neuroscience* **120,** 143–154
35. Ono, Y., Kinouchi, T., Sorimachi, H., Ishiura, S., and Suzuki, K. (1997) *J. Biochem.* **121,** 585–590
36. Perez, R. G., Soriano, S., Hayes, J. D., Ostaszewski, B., Xia, W., Selkoe, D. J., Chen, X., Stokin, G. B., and Koo, E. H. (1999) *J. Biol. Chem.* **274,** 18851–18856
37. Steinhilb, M. L., Turner, R. S., and Gaut, J. R. (2002) *J. Neurochem.* **80,** 1019–1028
38. Takahashi, K., Niidome, T., Akaike, A., Kihara, T., and Sugimoto, H. (2008) *Biochem. Biophys. Res. Commun.* **377,** 544–549
39. Lee, C. M., and Tannock, I. F. (2006) *Br J. Cancer* **94,** 863–869
40. Simon, S. M., and Schindler, M. (1994) *Proc. Natl. Acad. Sci. U.S.A.* **91,** 3497–3504
41. Rajendran, L., Schneider, A., Schlechtingen, G., Weidlich, S., Ries, J., Braxmeier, T., Schwille, P., Schulz, J. B., Schroeder, C., Simons, M., Jennings, G., Knölker, H. J., and Simons, K. (2008) *Science* **320,** 520–523
42. Yoon, I. S., Pietrzik, C. U., Kang, D. E., and Koo, E. H. (2005) *J. Biol. Chem.* **280,** 20140–20147
43. Cam, J. A., and Bu, G. (2006) *Mol. Neurodegener.* **1,** 8
44. Spoelgen, R., von Arnim, C. A., Thomas, A. V., Peltan, I. D., Koker, M., Deng, A., Irizarry, M. C., Andersen, O. M., Willnow, T. E., and Hyman, B. T. (2006) *J. Neurosci.* **26,** 418–428
45. Schmidt, V., Sporbert, A., Rohe, M., Reimer, T., Rehm, A., Andersen, O. M., and Willnow, T. E. (2007) *J. Biol. Chem.* **282,** 32956–32964
46. Marzolo, M. P., and Bu, G. (2009) *Semin Cell Dev. Biol.* **20,** 191–200
47. Borg, J. P., Ooi, J., Levy, E., and Margolis, B. (1996) *Mol. Cell. Biol.* **16,** 6229–6241
48. Lee, M. S., Kao, S. C., Lemere, C. A., Xia, W., Tseng, H. C., Zhou, Y., Neve, R., Ahlijanian, M. K., and Tsai, L. H. (2003) *J. Cell Biol.* **163,** 83–95
49. Sano, Y., Nakaya, T., Pedrini, S., Takeda, S., Iijima-Ando, K., Iijima, K., Mathews, P. M., Itohara, S., Gandy, S., and Suzuki, T. (2006) *PLoS One* **1,** e51

Biochemical and Biophysical Research Communications 399 (2010) 593–599

Contents lists available at ScienceDirect

Biochemical and Biophysical Research Communications

journal homepage: www.elsevier.com/locate/ybbrc

Reduction of amyloid β-peptide accumulation in Tg2576 transgenic mice by oral vaccination

Rika Ishii-Katsuno [a,1], Akiko Nakajima [a,1], Taro Katsuno [a,1], Jun Nojima [a,1], Eugene Futai [a], Noboru Sasagawa [a], Taiji Yoshida [b], Yuichiro Watanabe [a], Shoichi Ishiura [a,*]

[a] Department of Life Sciences, Graduate School of Arts and Sciences, The University of Tokyo, Japan
[b] Local Crop Research Team, National Agricultural Research Center for Tohoku Region, Iwate, Japan

ARTICLE INFO

Article history:
Received 26 July 2010
Available online 1 August 2010

Keywords:
Alzheimer's
Amyloid β-peptide
Oral vaccination
Transgenic mice
Green pepper

ABSTRACT

Alzheimer's disease (AD) is pathologically characterized by the presence of extracellular senile plaques and intracellular neurofibrillary tangles. Amyloid β-peptide (Aβ) is the main component of senile plaques, and the pathological load of Aβ in the brain has been shown to be a marker of the severity of AD. Aβ is produced from the amyloid precursor protein by membrane proteases and is known to aggregate. Recently, immune-mediated cerebral clearance of Aβ has been studied extensively as potential therapeutic strategy. In previous studies that used a purified Aβ challenge in a mouse model of AD, symptomatic improvement was reported. However, a clinical Alzheimer's vaccine trial in the United States was stopped because of severe side effects. Immunization with the strong adjuvant used in these trials might have activated an inflammatory Th1 response.

In this study, to establish a novel, safer, lower-cost therapy for AD, we tested an oral vaccination in a wild-type and a transgenic mouse model of AD administered via green pepper leaves expressing GFP-Aβ. Anti-Aβ antibodies were effectively induced after oral immunization. We examined the immunological effects in detail and identified no inflammatory reactions. Furthermore, we demonstrated a reduction of Aβ in the immunized AD-model mice. These results suggest this edible vehicle for Aβ vaccination has a potential clinical application in the treatment of AD.

1. Introduction

Alzheimer's disease (AD) is one of the major causes of chronic and progressive age-associated cognitive decline, with characteristic pathological hallmarks including extracellular senile plaques, intracellular hyperphosphorylated tau in neurofibrillary tangles, and brain weight loss [1,2].

Amyloid β-peptide (Aβ), which is reported to aggregate spontaneously, is the major constituent of the senile plaques in patients with AD. Aβ has been reported to accumulate on the outside of nerve cells or in the cerebral vascular walls. According to the amyloid cascade hypothesis, the gradual cerebral accumulation of soluble and insoluble assemblies of Aβ in the limbic and association cortices triggers a cascade of biochemical and cellular alterations that produce the clinical phenotype of AD. Therefore, soluble or insoluble Aβ is regarded as a therapeutic target of the progression of AD.

Aβ is generated by the sequential proteolytic processing of the amyloid precursor protein (APP) by membrane proteases. In human brains, the longer Aβ peptide, Aβ42, has a greater propensity to aggregate than the shorter Aβ40.

In 1999, a vaccination therapy to Aβ was developed as a novel therapeutic method against AD. These experiments employed APP transgenic mouse model of AD (PDAPP) mice, which overexpress mutant human APP and progressively develop senile plaques or neurofibrillary tangles in an age- and brain region-dependent manner. In the study, transgenic mice were immunized with synthesized Aβ42 either before (at 6 weeks of age) or after (11 months) the onset of neuropathologies. The study reported that the antibody titer against Aβ42 was elevated, and immunization of the young animals essentially prevented the development of senile plaques, neurofibrillary tangles, and neuritic atrophy. Treatment of the older animals also markedly reduced the extent and progression of these AD-like neuropathologies [3]. This reduction in the number of senile plaques was observed not only with active immunization but also with passive immunization [4] and with the mucosal immunization delivered via the nose [5].

Transgenic mouse models of AD, such as PDAPP mice, begin to display a learning disability derived from the cognitive disorder

* Corresponding author.
E-mail address: cishiura@mail.ecc.u-tokyo.ac.jp (S. Ishiura).
[1] These authors are equally contributed to this work.

0006-291X/$ - see front matter © 2010 Elsevier Inc. All rights reserved.
doi:10.1016/j.bbrc.2010.07.120

in a water maze test at around 15 months of age, but this learning disorder improves with the Aβ42 immunization [6–9]. In 2001, the Elan Corporation in the United States examined the clinical application of Aβ immunization. However, during the phase II trial, some patients presented with acute meningitis as a side effect after the second immunization, and this clinical test was suspended [10]. Adjuvants used in the muscular injection of the synthesized Aβ42 have high immunological activity and induce cell-mediated immune responses such as T-lymphocyte activation. In some cases, Aβ or APP-reactive killer T cells may have invaded the brain causing allergic meningitis. Despite the suspension of the clinical trial, some data suggest that the vaccination therapy may be effective for Aβ clearance [11]. Overall, these results indicate that safer and cheaper vaccination methods are needed, in particular those that do not require injection, strong adjuvants, and expensive synthesized peptides.

As for the safety of the vaccine, physiological immunoreactivity against the vaccine is of great importance. In the human body, immunoreactivity against "the self" is usually suppressed, a phenomenon called immunotolerance. "Self" immunotolerance is affected by the balance between Th1 and Th2 helper T cells. When the balance between Th1 and Th2 T cells changes and Th1 cells are activated, cellular reactions to "the self" increase, tending to give rise to autoimmune diseases such as meningitis. When Th2 cells are activated, antibody production is induced and anti-inflammatory cytokines are released to alleviate the inflammation induced by Th1 cells. Safer vaccine therapies that induce the Th2 reaction via mucosal immunization are now being tested in animal models. In mucosal immunization, immune activity tends to be feeble, immunotolerance can be induced, and adjuvants delivered with the target antigen proteins must be taken into consideration. In an experiment in which a DNA vaccine was administered via the nose, Kim et al. delivered Aβ and adenovirus vectors coding granulocyte colony-stimulating factor (G-CSF) as the adjuvant, and effective elevation of anti-antibody titer and continual induction of Th2 reaction was reported [14].

Many studies of vaccination therapy for AD have been conducted, such as subcutaneous or nasal mucosal vaccination using synthetic peptide or DNA [5,15,16], but oral vaccination using an edible, virally transduced plant as a vehicle has some benefits [17,18]. First, because only the target subunits or fragments are expressed, and not all the pathogenic virus or proteins, it is a safer vaccine. Furthermore, purification of the target protein and cold storage are not required, and the cost is low. Plant biotechnology provides methods for introducing animal genes into plants.

In this study, we tested a plant-based vaccination therapy in an animal model of AD. We expressed green fluorescent protein (GFP)-conjugated Aβ in pepper leaves using a plant virus and fed the leaves to wild-type or transgenic mice. We used the cholera toxin B subunit (CTB) as the oral adjuvant. CTB suppresses Th1 cell reactivity and is known to form a pentamer, binding to GM1 gangliosides on the cell surface. Then we examined the immunological reaction in mice and checked the effectiveness and safety of this plant-based vaccination.

We succeeded in stably expressing GFP-conjugated Aβ in green pepper leaves using a plant virus, TocJ. Oral vaccination of wild-type and Tg2576 transgenic mice resulted in the elevation of Aβ antibody titer without significant side effects.

2. Materials and methods

2.1. Mice

We used female Tg2576 transgenic mice (670th amino acid of APP mutated from Lys to Asn, and 671st from Met to Leu), a model of Swedish familial AD, and female wild-type B6 mice.

2.2. Plants

For the plant-based vaccine, we used leaves of *Capiscum annuum* var. angulosum virally transduced with GFP-conjugated Aβ42 using a plant virus, TocJ [18,21]. Viral transduction with GFP alone was used as a negative control.

2.3. Quantification of Aβ expression in leaves of Capiscum annuum var. angulosum

The leaves were suspended in phosphate-buffered saline (PBS), homogenized, and centrifuged at 10,000*g* for 10 min (4 °C), then the supernatant was separated from the pellet. Protein samples were separated on 10% sodium dodecyl sulfate–polyacrylamide gel electrophoresis (SDS–PAGE) gels, transferred to polyvinylidene fluoride (PVDF) membranes (2 mA/cm^2 for 90 min), blocked with 5% skim milk for 60 min, and incubated in the mouse monoclonal antibody 6E10 at 4 °C overnight. Blots were then incubated with a horseradish peroxide (HRP)-conjugated secondary antibodies at room temperature for 10 min and then at 37 °C for 45 min. For detection and analysis of the luminescence, we used a lumino-image analyzer (Fujifilm, Tokyo, Japan).

2.4. Preparation of the leaves for immunization

The quantity of green pepper leaves administered to each mouse was adjusted to deliver 60 μg of Aβ. Samples for subcutaneous injection were prepared as follows: the green pepper leaves were suspended in PBS, centrifuged at 10,000*g* for 10 min (4 °C), and the supernatant was added to an equal volume of Freund's adjuvant and stirred to form an emulsion. Samples for oral administration were prepared as follows: crushed green pepper powder stored in liquid nitrogen was mixed with CTB (10 μg per mouse) in a 5% sucrose solution.

2.5. Mouse immunization

For subcutaneous immunization, each mouse was anesthetized with diethyl ether and injected with 100–200 μL of extract at several points using a 21G needle. For oral immunization, the mixture was orally delivered by gastric intubation.

We examined three groups of wild-type B6 mice. Five wild-type mice vaccinated orally with GFP-only served as negative controls. The rest of the wild-type mice were immunized with GFP-Aβ42 either subcutaneously ($n = 5$) or orally ($n = 6$). All wild-type mice received doses of vaccine biweekly from 3 to 11 months of age. Two weeks after a booster given at 11 months, whole blood was collected from the heart.

We examined three groups of Tg2576 mice. Ten Tg2576 mice vaccinated orally with GFP-only served as negative controls. The rest of the transgenic mice were immunized with GFP-Aβ42 either subcutaneously ($n = 8$) or orally ($n = 10$). All transgenic mice received doses of vaccine biweekly from 5.5 to 18 months of age. Two weeks after a booster at 18 months, whole blood was collected from the heart. Other than during vaccine dosing, animals were fed regular mouse chow during the entire experiment. All animals were housed 3–5 to a cage and maintained on ad libitum food and water with a 12 h light/dark cycle.

2.6. Quantification of the anti-Aβ antibody titer with ELISA

Well plates were coated with Aβ42 dissolved in 0.15 M ammonium solution and then washed five times with wash buffer (0.45% NaCl and 0.05% Tween 20). Next, the plates were blocked with 3% skim milk for 30–60 min at room temperature and washed four times.

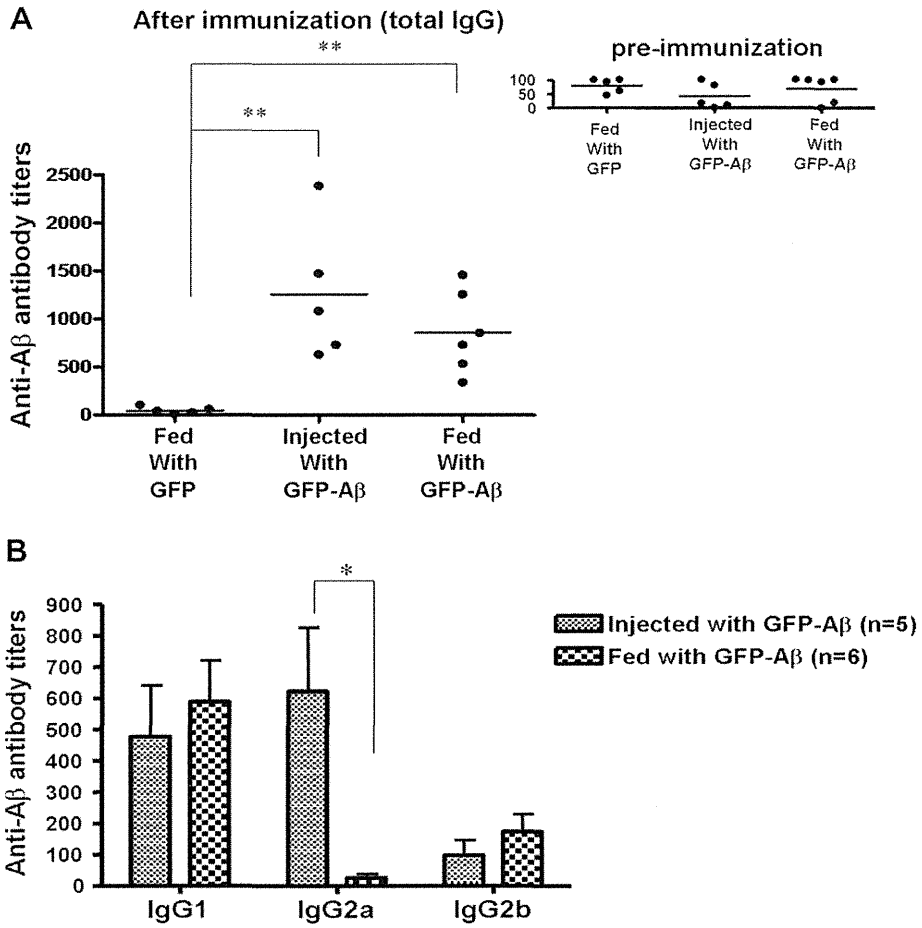

Fig. 1. (A) Elevation of the anti-Aβ titer in wild-type B6 mice. The antibody titer of each wild-type B6 mouse is shown in this figure ($^{**}P < 0.01$). Mice fed GFP-expressing leaves served as a control. (B) IgG isotyping of anti-Aβ antibodies in wild-type B6 immunized mice. Serum collected from GFP-Aβ-treated mice was used for IgG isotyping of anti-Aβ antibodies. Anti-Aβ antibody titers of each IgG isotype are shown for each condition. Mean ± SE. $^{*}P < 0.05$.

Blood plasma samples were diluted 10–10^5 times. Monoclonal anti-Aβ antibody 6E10 was diluted 10,000–160,000 times as a positive control. Each sample as applied to a well and incubated at 37 °C for 1 h. After washing six times, each well was blocked at room temperature for 30 min with 3% skim milk and again washed five times. Wells were incubated with an HRP-conjugated secondary antibody at 37 °C for 1 h and washed 10 times. To complete the enzyme-linked immunosorbent assay (ELISA), wells were incubated with tetramethylbenzidine (TMB) substrate at room temperature in the dark. After sufficient color reaction occurred, 2 M phosphate buffer stopped the reaction. We measured the absorbance at 450 nm with a spectrophotometer and calculated antibody titers using the statistics software, PRISM version 4.

2.7. Aβ quantification in Tg2576 mouse brains using sandwich ELISA

At the end of the vaccination protocol, we removed the brains of Tg2576 mice and homogenized one hemisphere in with Tris-buffered saline (TS) and centrifuged this sample at 4 °C and 200,000g for 20 min. The supernatant was used as the soluble fraction. After the pellet was washed with TS, we homogenized the pellet with 6 M guanidine–Tris buffer. After sonification at room temperature for 30 s, the sample was incubated for 1 h at room temperature and then centrifuged at 4 °C and 200,000g for 20 min. We made a 1:12 dilution of the sample in sandwich ELISA dilution buffer. The precipitate was regarded as the insoluble fraction.

We measured the amount of Aβ42 in each brain using a sandwich ELISA kit (Wako, Osaka, Japan). First, we incubated Aβ42 peptide standards and brain extract samples at 4 °C overnight on microplates coated with a monoclonal antibody raised against the human Aβ42 N-terminus. The plate was washed with wash buffer five times, and then incubated at 4 °C overnight with BC05, a HRP-conjugated antibody raised against the Aβ42 C-terminus. After five washes, a color reaction was carried out at room temperature in the dark and then stopped after 30 min. We measured the absorbance at 450 nm and calculated the concentration of Aβ42 from the standard curve.

2.8. Immunostaining of Tg2576 mouse brain slices

We fixed the remaining brain hemisphere with 4% paraformaldehyde overnight. Then, the brains were embedded in paraffin, sliced at 4 μm thickness, and immunostained using the 6E10 primary antibody and a diaminobenzidine (DAB) color reaction.

3. Results

3.1. Quantification of Aβ expression in plant leaves

We performed SDS–PAGE and Western blotting for green pepper leaf extracts in PBS. We used the mouse monoclonal antibody 6E10 as the primary antibody to detect Aβ. Then we quantified the expression of Aβ using synthesized mouse IgG as the protein standard. The amount of Aβ was 100–600 μg for 1 g of plant leaves, depending on the preparation.

3.2. Production of anti-Aβ antibodies in wild-type B6 mice

To study the course of antibody production after vaccination and the precise immunological response, subcutaneous or oral immunization of wild-type B6 mice was performed starting at 3 months of age and continued for 8 months. The vaccine was administered once every 2 weeks. We quantified and calculated the serum anti-Aβ antibody titer (Fig. 1A). Compared to the GFP controls, serum anti-Aβ titer was significantly elevated in the groups receiving GFP-Aβ.

3.3. IgG isotyping in wild-type mice

To check the safety of the food vaccination, we determined the isotype of anti-Aβ antibodies produced in the serum and checked for inflammatory reactions in GFP-Aβ vaccinated mice (Fig. 1B). IgG1 and IgG2b are known to be the non-inflammatory Th2 isotype IgGs and IgG2a is the inflammatory Th1 isotype IgG. This latter isotype is used as a marker of inflammation. We found that the amount of IgG2a was significantly reduced in mice administered the vaccine orally compared to those receiving the subcutaneous injection.

3.4. Anti-Aβ antibody production in a transgenic mouse model of AD

To examine whether the food Aβ vaccination was effective in a mouse model of AD in which Aβ accumulates in an age-dependent manner, we immunized Tg2576 mice subcutaneously or orally. The mice received the vaccine biweekly from 5 .5 to 16.5 months of age. Samples were collected at the age of 18 months. We first scored the anti-Aβ antibodies and calculated the antibody titers (Fig. 2A). Compared to control mice treated with GFP-only orally, serum anti-Aβ antibody titer was significantly elevated in GFP-Aβ-treated mice. The increase in titer was the same for those injected with vaccine.

3.5. IgG isotyping in Tg2576 mice

To examine the safety of food vaccination in Tg2576 mice, we examined anti-Aβ antibody isotypes and inflammatory reaction in the GFP-Aβ-treated mice (Fig. 2B). Compared to the subcutaneous injection group, serum IgG2a was significantly reduced in the oral administration group.

3.6. Aβ burden in the mouse brains

We homogenized one hemisphere of the brain in Tris-buffered saline, centrifuged the sample, homogenized the pellet in 6 M guanidine–Tris buffer, and quantified the amount of Aβ with sandwich ELISA (Fig. 3A). In the GFP-Aβ-treated mice, the amount of intracerebral Aβ was significantly reduced compared to control mice. However, the amount in the insoluble Aβ samples of subcutaneously injected mice was not significantly different from that of control mice.

The other hemisphere of the brain was used for immunological staining with anti-Aβ antibody 6E10 (Fig. 3B). Fewer senile plaques were observed in GFP-Aβ-treated mice than in control mice.

4. Discussion

The hypothesis that Aβ vaccination should prevent senile plaque formation was raised in an experiment by Schenk et al. The

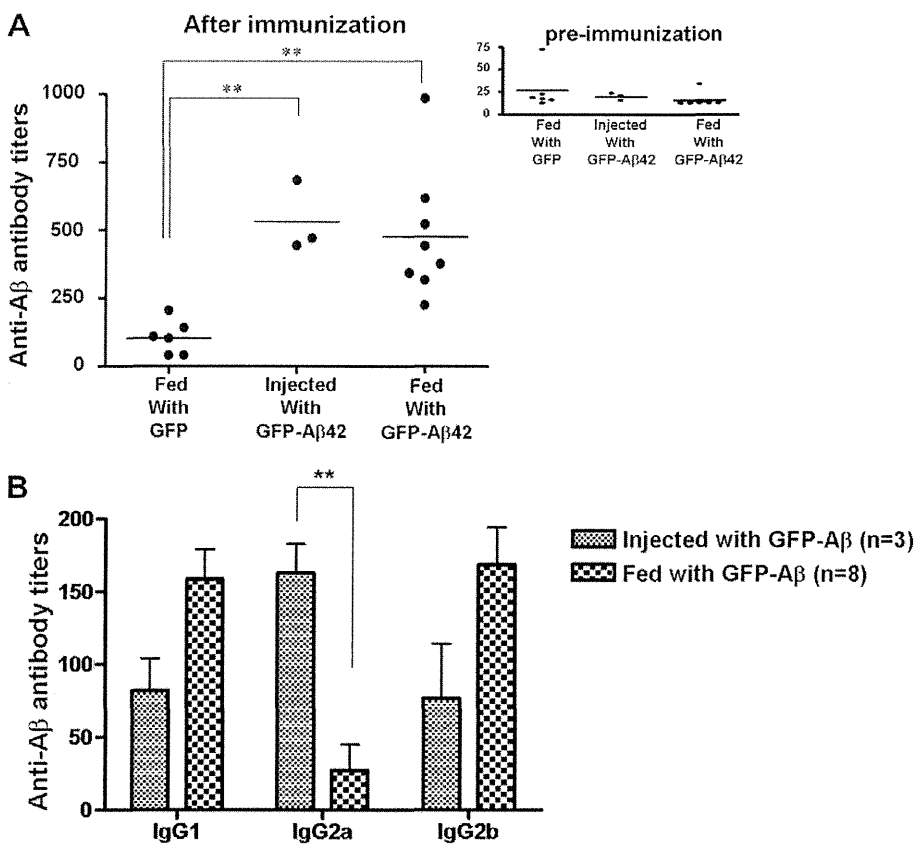

Fig. 2. (A) The anti-Aβ antibody titer is elevated in Tg2576 mice. The titer of antibodies against the Aβ protein increased after immunization. $^{**}P < 0.01$. (B) IgG isotyping of anti-Aβ antibodies in immunized Tg2576 mice. Serum collected from GFP-Aβ-treated mice was used for IgG isotyping of anti-Aβ antibodies. Anti-Aβ antibody titers of each IgG isotype are shown for each condition. Mean ± SE. $^{**}P < 0.01$.

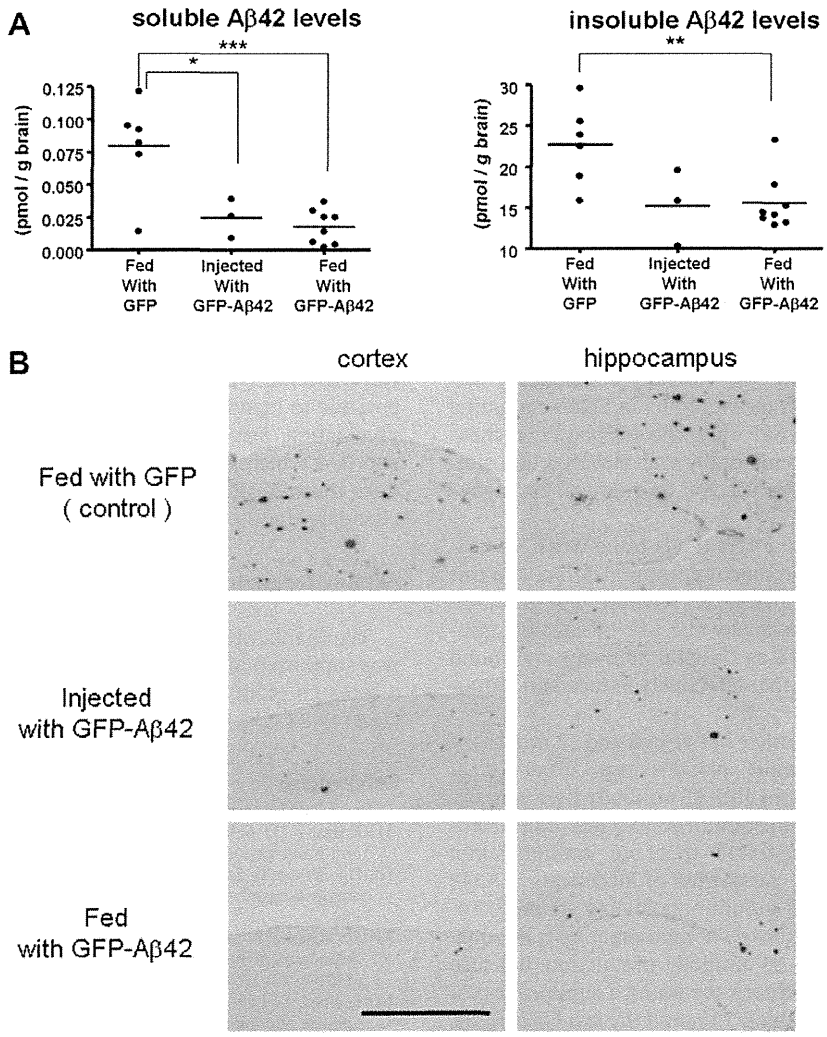

Fig. 3. (A) Intracerebral Aβ42 content in Tg2576 mice. A plot of the concentration of Aβ42 per 1 g of brain for each mouse. (a) The level of soluble Aβ42. (b) The level of insoluble Aβ42. (B) Immunostaining of Tg2576 mouse brains (left: cortex; right: hippocampus). Bar = 1 mm.

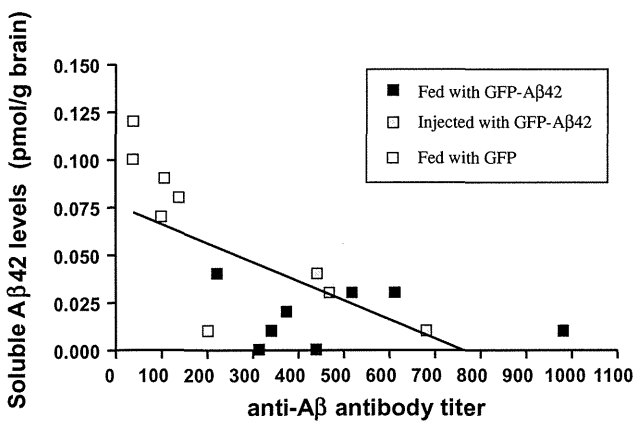

Fig. 4. The anti-Aβ antibody titer correlates with the level of soluble intracerebral A 42 in Tg2576 mice. These data were recalculated from those of Figs. 2A and 3A. $r = -0.686$, $p = 0.0023$.

authors put several kinds of antibodies against Aβ on frozen brain slices with senile plaques either from transgenic mice or from human patients with AD. Then the brain slices were incubated with a reagent containing microglia and phagocytes. If the antibodies were specific to Aβ, the microglia phagocytized Aβ on the brain section. This did not happen with antibodies to other proteins. These results supported the amyloid phagocytizing hypothesis that anti-Aβ antibodies bind to Aβ and then Aβ is phagocytized by microglia via Fc receptors [4]. When a monoclonal antibody against Aβ, m266, was peritoneally injected into transgenic mice, the amount of senile plaques was reduced in the brain and monomers and dimers of Aβ in the blood were elevated 1000 times over control 24 h after the injection. These findings also support the sink hypothesis that anti-Aβ antibodies mainly bind to and promote the clearance of peripheral Aβ, causing the Aβ to be drawn out of the central nervous system [12,13].

Most vaccines are administered by hypodermic injection. The antigens are either inactivated proteins, attenuated viruses, or bacteria. The protein antigen itself does not invite infection and is safe. These vaccines must be stored at cold temperatures and can be costly. Other vaccines are administered by mucosal application. Mucosal immunization utilizes the alimentary tract-associated lymphoid system. This mucosal epidermis is the first place from where some external antigens enter the body, and many lymphocytes are in the mucosal lymphoid tissue. In the mucosal immunity strategy, these lymphoid tissues are needed to accept only the target antigen specifically and effectively. The vaccination method used in the present study utilized the nasal mucous membrane-associated lymphoid system.